14 U-Th-Pb Dating of Phosphate Minerals

T. Mark Harrison

Research School of Earth Sciences
The Australian National University
Canberra, A.C.T. 0200 Australia

Elizabeth J. Catlos

School of Geology
Oklahoma State University
Stillwater, Oklahoma 74078

Jean-Marc Montel

LMTG-Minéralogie UMR
CNRS 5563, 39 allées J. Guesde
31000 Toulouse, France

BACKGROUND

Introduction

The dominant occurrence of phosphate minerals in crystalline rocks is as accessory phases, most notably apatite, monazite, and xenotime. Because these minerals tend, to varying degrees, to partition U and Th into their structures they can often contain the majority of those elements in a rock. These three phases, again to varying degrees, tend not to incorporate significant amounts of Pb during crystallization and thus were early candidates for utilization as U-Th-Pb geochronometers.

The ideal U-Th-Pb geochronometer would be a phase that is stable over all possible environmental conditions and is quantitatively retentive of parent and daughter isotopes. In fact, the silicate zircon comes reasonably close to meeting these criteria. Zircon has a broad stability field, is refractory under a wide variety of geologic environments (e.g., weathering, sedimentary transport, anatexis, and metamorphism), and can be highly retentive of daughter products in the U-Th-Pb decay system. However, the limit of zircon as an ideal chronometer lies only in its limited resistance to auto-irradiation damage that can render it metamict. The phosphate minerals apatite, monazite and xenotime have a more restricted range of stability and, to varying degrees, are incompletely retentive of Pb under crustal conditions, but they are resilient to radiation damage. Thus interpretation of results from these geochronometers requires a greater understanding of their structure, stability, and kinetic properties than does zircon. This chapter is aimed at providing the reader with an introduction to those characteristics that will facilitate interpretation of the occasionally problematic nature of phosphate U-Th-Pb dating results.

The U-Th-Pb dating system

U and Th decay. Nuclei approaching one hundred protons are unstable because the strong nuclear force, which acts to hold neutrons and protons together, is about 100 times greater than electromagnetic repulsion. Both uranium (92 protons) and thorium (90 protons) decay by emission of a ^{4}He nucleus (or α particle), which lowers the coulomb energy but changes the nuclear binding energy little. In certain cases, the intermediate daughter product is unstable with respect to β^- decay and transmutes to an isobar closer to the valley of beta stability.

Both long-lived isotopes of uranium, ^{238}U and ^{235}U, decay to isotopes of Pb with

1529-6466/00/0048-0014$05.00 DOI: 10.2138/rmg.2002.48.14

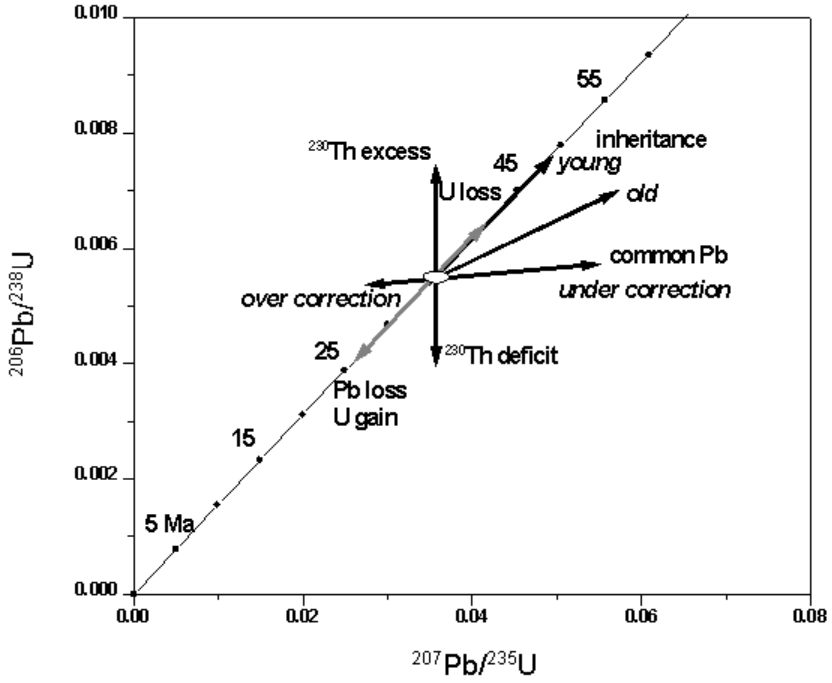

Figure 1. Concordia diagram illustrating misbehavior in the U-Th-Pb system that is relevant to U-Pb dating. Arrows show how concordant data can be affected by inheritance, Pb loss, disequilibrium, and common Pb (Pb°) corrections.

concordia curve. Continuous diffusive Pb loss results in a broadly linear array which resembles that of episodic Pb loss, cautioning against ascribing significance to a lower intercept unless independent evidence exists for a geologic event at that time (Faure 1986). Analysis of minerals that experienced and recorded complicated metamorphic histories can result in discordia lines with lower intercepts that have no geological meaning due to mixed ages.

Inheritance presents another complication that arises when protolith is incompletely consumed during a rock forming process and the restitic phase retains daughter Pb. Such occurrences are likely in crustal melts as solubilities of phosphate minerals such as apatite and monazite are generally low (Harrison and Watson 1984, Rapp and Watson 1986). Because the solidus temperature for many crustal magmas is higher than early estimates of closure temperature for Pb in monazite, inheritance of monazite in igneous rocks was once believed to be quite rare. However, numerous studies have documented the survival of restitic monazite in granitoids, dispelling this notion (Copeland et al. 1988, Harrison et al. 1995, Edwards and Harrison 1997). The preservation of inheritance in monazite saturated crustal magmas appears to be due to short timescales of crustal melting and the high degree of retentivity of Pb in monazite (Copeland et al. 1988, Montel 1993, Cherniak et al. 2000).

Incorporation of a restitic mineral containing radiogenic Pb (Pb*) during mineral growth in a melt will result in anomalously old ages that plot to the right of the concordia curve (Fig. 1). A more complicated case arises when a mineral has inherited Pb sometime in the past and then lost Pb more recently, potentially resulting in concordant data, which yield meaningless ages (e.g., Deniel et al. 1987). In the case of new mineral growing around an inherited core, bulk analysis methods will yield a range of ages, reflecting mixing between two or more age components. On a concordia diagram this would manifest itself as a mixing line (2 components) or mixing array (multiple components).

As we note later, such a mixture is potentially resolvable using (or combining isotope dilution with) a technique that provides high spatial resolution, such as ion or electron microprobe analysis, or laser ablation-inductively coupled plasma-mass spectrometry. Disequilibrium between different nuclides in the ^{238}U or ^{235}U decay schemes can seriously complicate young U-Pb age data interpretation (Schärer 1984). For example, monazite contains abundant ThO_2 (1 to >30 wt %) (Overstreet 1967, Deer et al. 1992, Van Emden et al. 1997) and has a marked preference for Th compared to U, thus often incorporating a component of ^{230}Th, a relatively short-lived intermediate daughter isotope in the ^{238}U decay chain. The decay of ^{230}Th results in unsupported ^{206}Pb, anomalously high $^{206}Pb/^{238}U$, and thus data plot above the concordia curve (Schärer 1984). On a concordia diagram, excesses in intermediate decay products in the ^{238}U chain will move data up parallel to the $^{206}Pb/^{238}U$ axis (Fig. 1). Schärer (1984) first documented and corrected for this so-called reverse discordance in Himalayan monazite (see Fig. 2), which has subsequently been widely recognized (e.g., Schärer et al. 1986, Parrish and Armstrong 1987). Xenotime also presents a problem due to its lack of incorporation of ^{230}Th and resulting deficiency of ^{206}Pb, whereas monazite can incorporate ^{231}Pa, resulting in unsupported ^{207}Pb (Schärer 1984).

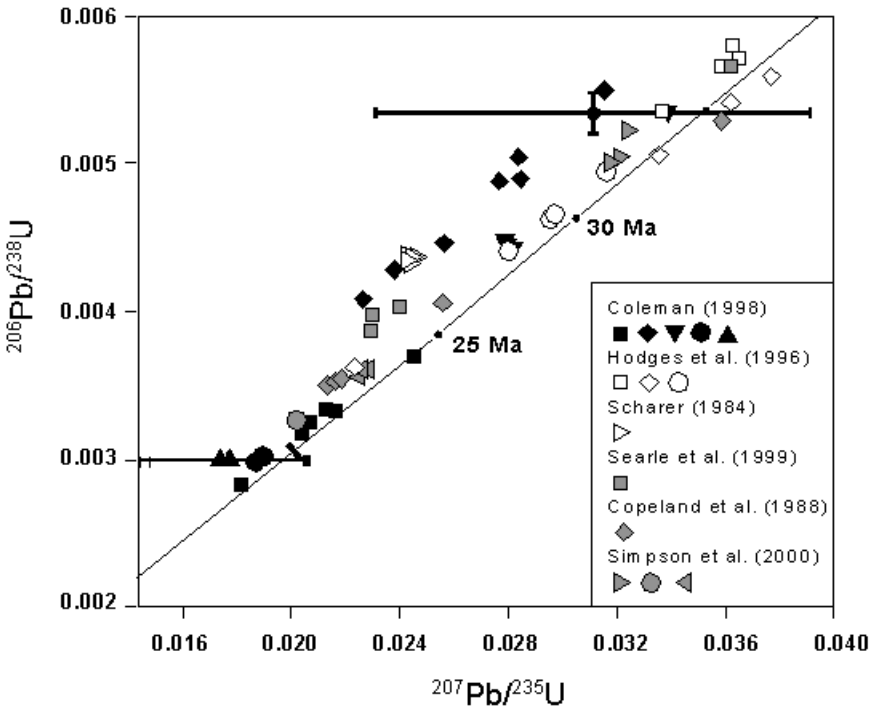

Figure 2. Concordia diagram of Himalayan monazite grains. References listed in the key. Note that a remarkable number these monazite grains show reverse discordance, consistent with incorporation of excess ^{206}Pb.

Complications due to inheritance, Pb loss, and disequilibrium highlighted in the above discussion can be particularly problematic for bulk or chemical measurement methods, but other techniques have their own drawbacks. For example, U-Pb ion microprobe data can be subject to calibration shifts that move a concordant data point along a line with a slope proportional to its $^{207}Pb/^{206}Pb$ age. Data can also be pulled to the left or right of concordia by over or under-correcting for common Pb (Pb^0) (Gilley 2001).

Note that ^{232}Th-^{208}Pb dating of monazite is insensitive to problems arising from disequilibrium of Pb because secular equilibrium among the intermediate daughter

isotopes is reached within ~30 years, making it unlikely that monazite could contain unsupported ^{208}Pb* (Harrison et al. 1995). In addition, the high ThO_2 concentrations in monazite result typically in high levels of ^{208}Pb*.

Early dating attempts. Because certain phosphate minerals strongly concentrate radioactive elements, early twentieth century geochronologists recognized their value. Monazite was an early candidate for U-Th-Pb dating (Fenner 1928, Nier et al. 1941) whereas the dating of apatite (Aldrich et al. 1955, Tilton et al. 1955) and xenotime (Lyakhovich 1961, Köppel and Grünenfelder 1975) were not attempted until later. Numerous methods were developed to obtain ages of phosphate minerals. Radiographic photos were used to document the distribution of radioactive elements within large monazite crystals and to ascertain the extent of alteration (see Fenner 1932, Marble 1935). Monazite grains so selected were washed with nitric acid to eliminate contamination or alteration products and then reacted with acids to isolate Th, U, and Pb (e.g., Fenner 1928, 1932). Prior to isotopic determinations (e.g., Nier et al. 1941), the fundamental equation for calculating ages was

$$[\log(U + 0.38\ Th + 1.156\ Pb) - \log(U + 0.38\ Th)]/(0.434\ \lambda)$$

where U, Th, and Pb are measured concentrations and λ is the total U decay constant, then assumed to be 1.5×10^{-11}/yr (Fenner 1932, Marble 1935). Constants arise in this equation via assumptions made about the equivalence of Th to U in radioactive decay. Although this age equation incorporated U decay, monazite was considered as a primarily Th-bearing phase and U was used as a proxy for alteration (Fenner 1928, Marble 1935). Uranium in monazite posed a problem for early geochronologists, who speculated that the element could be "brought in by circulating waters from adjacent uranium minerals" (Fenner 1932). Today, monazite is commonly dated using the U-Pb method (e.g., Schärer 1984, Copeland et al. 1988, Parrish and Tirrul 1989, Hodges et al. 1996, Parrish and Hodges 1996, Simpson et al. 2000) and more recently by Th-Pb (e.g., Wang et al. 1994, Harrison et al. 1995, Grove and Harrison 1999, Catlos et al. 2001, 2002a).

Monazite was also analyzed using "the Larsen method," in which the total Pb content was compared to measured alpha activity (Larsen et al. 1949, Gottfried et al. 1959, Sivaramakrishnan and Venkatasubramaniam 1959). Although the Larsen method was viewed as "considerably less precise than any of the isotopic methods currently employed in age work" (Gottfried et al. 1959), a large number of Pb-α age determinations could be made rapidly and inexpensively. Apatite was also analyzed by the Larsen method (Larsen et al. 1949) and later by U-Th-Pb dating (Aldrich et al. 1955, Tilton et al. 1955, Iskanderova and Legiyerskiy 1966, Vinogradov et al. 1966).

The existence of monazite and uraninite in the same geologic setting led to age comparisons and the recognition that uraninite was incompletely retentive of daughter Pb (Fenner 1932, Holmes et al. 1949, Ahrens 1955). The geochronologic significance of xenotime ages were evaluated in relation to monazite and Rb-Sr mica ages from the same or neighboring rocks (e.g., Köppel and Grünenfelder 1975).

When the capability arose to measure Th, U, and Pb isotopes (Nier 1939), it was recognized that many monazites yield different U-Pb and Th-Pb ages. Table 2 is a compilation of monazite age data obtained between 1941-1957. Tilton and Nicolaysen (1957) report "gross discrepancies" between individual isotopic ages that "greatly exceed experimental errors" and speculate that although "Pb loss is a more plausible explanation for low U-Pb and Th-Pb ages than U or Th gain…it is very difficult to give a definite proof for this hypothesis." Discordant monazite ages were attributed to Pb diffusion via extended time at elevated temperatures or prolonged chemical reactions occurring at varying rates and involving different agents (see Shestakov 1969). In natural samples,

half-lives of 4.4 Ga and 700 Ma (see Table 1), respectively, through a complex chain of intermediate daughter isotopes (Faure 1986). The overall decay relationships are:

$^{238}U \rightarrow {}^{206}Pb + 8\ \alpha + 6\ \beta^- + 47.4$ MeV

$^{235}U \rightarrow {}^{207}Pb + 7\ \alpha + 4\ \beta^- + 45.2$ MeV

Table 1. Solutions to U-Th-Pb age equations.

System	*Decay constant (Ma^{-1})*	*Solution*
$^{238}U \rightarrow {}^{206}Pb$	1.55125×10^{-4}	$^{206}Pb = {}^{238}U \cdot \left(e^{\lambda_{238} t} - 1\right)$
$^{235}U \rightarrow {}^{207}Pb$	9.8585×10^{-4}	$^{207}Pb = {}^{235}U \cdot \left(e^{\lambda_{235} t} - 1\right)$
$(^{207}Pb/^{206}Pb)^*$		$\left(\frac{^{207}Pb}{^{206}Pb}\right)^* = \frac{1}{137.88}\left(\frac{e^{\lambda_{235} t} - 1}{e^{\lambda_{238} t} - 1}\right)$
$^{232}Th \rightarrow {}^{208}Pb$	4.9475×10^{-5}	$^{208}Pb = {}^{232}Th \cdot \left(e^{\lambda_{232} t} - 1\right)$

In order that the U-Pb date corresponds to the age of mineral formation, the series of intermediate daughter activities must be in secular equilibrium, which occurs after five half-lives of the intermediate isotope have elapsed. Most of the intermediate daughter isotopes are short-lived (i.e., half-lives of <10,000 years), but ^{234}U (in the ^{235}U decay chain) and ^{230}Th (in the ^{238}U decay chain) have half-lives of 247,000 and 76,000 years, respectively, thus requiring up to ~1 Myr for attainment of secular equilibrium. Therefore, secular equilibrium cannot be considered instantaneous over geologic time, and element partitioning during growth leads to preferential exclusion or uptake of intermediate daughters resulting in, respectively, daughter product deficiencies or excesses.

The single long-lived isotope of thorium, ^{232}Th, decays to ^{208}Pb (Table 1) with a half-life of 14 Ga through a series of intermediate daughters via the relationship:

$^{232}Th \rightarrow {}^{208}Pb + 6\ \alpha + 4\ \beta^- + 39.8$ MeV

Unlike uranium, intermediate daughter isotopes from ^{232}Th decay all have short half-lives such that secular equilibrium is achieved across the chain within ~30 years.

The concordia plot. Because uranium isotopes are unlikely to be fractionated in nature, the paired decay of ^{238}U and ^{235}U permits the two decays systems to be plotted together (Fig. 1) yielding the so-called concordia plot (Wetherill 1956). The potential advantage of such a plot is that a single stage of open system behavior can in principle be recognized and corrected. For ancient samples, this approach appears to work well. However, more youthful samples are problematic and phosphates in particular can be pathological in this regard. Because of this, we focus particularly on the behavior of young (i.e., <100 Ma) phosphates.

Pb loss (or U gain) has the effect of moving data off concordia along a line whose lower intercept reflects the age of the disturbance (Fig. 1). For recent Pb loss (or U gain), that intercept is the origin. A sample that has experienced minor Pb loss will plot close to its origin on the concordia curve, while one that has lost more Pb will move down a discordia line towards the lower intercept. U-Pb ages of young samples can be difficult to interpret because the trajectory of Pb loss may not be resolvable from concordia. In the case of multiple Pb loss events, the data will fan out from the upper intercept on the

Michot and Deutsch (1970) invoked Pb loss via recrystallization and episodic metamorphism to explain age discrepancies.

To ascertain the source of the monazite Th-Pb and U-Pb age difference, analytical techniques were evaluated for isotopic fractionation (e.g., Burger et al. 1967) and diffusion experiments were performed (e.g., Tilton 1960, Shestakov 1969).

Table 2. Mid-twentieth-century monazite age data (Ma)[a]

Sample name (locality)	*^{238}U-^{206}Pb*	*^{235}U-^{207}Pb*	*^{207}Pb-^{206}Pb*	*Th-^{208}Pb*	*% diff.*[b]
Ebonite Claims (S. Rhodesia)	2640	2670	2700	2640	1
Ebonite Claims (S. Rhodesia)	2620	2620	2620	2640	-1
Yadiur (India)	1410	1820	2330	1800	1
Goodhouse (S. Africa)	930	915	880(60)[b]	900	2
Steenkampskraal (S. Africa)	1080	nr[c]	nr	990	9
Soniana (India)	635	697	913	611	14
Mount Isa (Australia)	nr	nr	1160	1000	16
Jack Tin Claims (S. Rhodesia)	2210	2460	2660	1940	27
Houtenbek (S. Africa)	1400	1230	930(50)	940	31
Brown Derby (Colorado)	1590(30)	1420(10)	1170(50)	995(25)	43
Huron Claim (Canada)	3180	2840	2600	1830	55
Irumi Hills (N. Rhodesia)	1990	2330	2640	1380	69
Las Vegas (New Mexico)	1730	1560	1340	770	103
Antsirabe (Madagascar)	1370	1850	2450	610	203

a. Note most results have errors of 3-5% unless otherwise indicated (Neir et al. 1941, Holmes et al. 1949, Holmes, 1954, 1955; Holmes and Cahen 1955, Aldrich et al. 1956, Tilton and Nicolaysen 1957).

b. To quantify the difference between the ^{235}U-^{207}Pb and Th-Pb ages, we used {[(^{235}U-^{207}Pb age)-(Th-^{208}Pb age)]/(Th-^{208}Pb age)}*100. For the Steenkampskraal monazite, ^{238}U-^{206}Pb age and Mount Isa ^{207}Pb-^{206}Pb age were used instead of ^{235}U-^{207}Pb age. Note in many cases Th-Pb ages are younger than the U-Pb ages.

c. "nr" = not reported.

Despite potential problems with method, mineral ages of phosphates were used to address geologic problems. Apatite could be analyzed to understand crystallization history during metasomatism (e.g., Iskanderova and Legiyerskiy 1966). Xenotime and monazite U-Th-Pb ages were applied to problems regarding the timing of Alpine metamorphism (e.g., Köppel and Grünenfelder 1975). Monazite ages from the African continent were used to constrain the origin of life on Earth to ~2.6 Ga (Holmes 1954).

MINERAL STRUCTURE AND RADIATION DAMAGE CONSIDERATIONS

Monazite

Mineral structure. Monazite has an ABO_4 stoichiometry, where A-site is occupied by large cation, such as rare earth elements (REE^{3+}), Ca^{2+}, Th^{4+}, and B-site contains small, tetrahedrally coordinated cations, such as P^{5+}. The structure of monazite is comprised of chains of alternating PO_4 tetrahedra, and nine-fold coordinated REE in the A site (e.g., Ni et al. 1995, and Boatner, this volume). All REE are accepted in the A site, although, as far as pure end-members are concerned, only $LaPO_4$ to $GdPO_4$ have the monazite structure at room temperature.

The incorporation of U and Th is accommodated in the REE-site via two substitutions (Burt 1989, van Emden et al. 1997, Förster 1998a): the huttonitic

substitution $REE^{3+}P^{5+}=Th^{4+}Si^{4+}$ and the brabantitic (or cheralitic) substitution $2REE^{3+}=Ca^{2+}Th^{4}$. Corresponding end-members are huttonite ($ThSiO_4$) and brabantite ($Ca_{0.5}Th_{0.5}PO_4$). The same substitution accounts for U but the corresponding end-members have not been found. Experimental studies have shown that the $LaPO_4$-$Ca_{0.5}Th_{0.5}PO_4$ and $LaPO_4$-$Ca_{0.5}U0_{.5}PO_4$ solid solutions are continuous (Podor et al. 1995, Podor and Cuney 1997). Some data suggest also that the $LaPO_4$-$ThSiO_4$ solid solution is continuous (Peiffert and Cuney 1999). Experiments show that the A site can accept various divalent cations instead of Ca including Cd, Sr, Pb, and Ba (Montel et al. 2002).

Because of its ability to accept U and Th, monazite is one of the most radioactive minerals after uraninite, thorianite or thorite. It is the most *common* radioactive mineral (Overstreet 1967), and in many rocks the main host of U and Th. The possibility for monazite to accept Pb in the same site as U and Th is obviously important for geochronology. Pb* produced by U and Th has a place in the structure (Quarton et al. 1984). Therefore there is a not a natural tendency for Pb to be released from monazite, as might be anticipated by considering the structure of zircon. Another consequence of the ability of monazite to incorporate various ions is that, in the three U and Th decay chains, most elements can be incorporated in the A site. If all actinides and a small amount of Ra (because Ba is favourably partitioned) can be accepted in monazite, all elements with half-lives greater than about one year are incorporated in the mineral structure. This suggests that at any moment in the radioactive decay chains of U and Th, there is little tendency for any intermediate decay products to escape from the mineral structure.

Radiation effects. Alpha decay is the primary cause of radiation damage in minerals. For example, ^{232}Th produces an alpha particle and a recoil nucleus of ^{228}Ra. The total energy of this decay is 4 MeV, and both the alpha particle and recoil nucleus are ejected from their initial lattice position in opposite directions (see Ewing 1994). The light alpha particle loses most of its energy by ionization along a 10,000-nm-long path, and its effect on the structure is small. In contrast, the recoil nucleus is big and heavy and displaces many atoms along a ~10 nm path, severely damaging the crystal lattice. Although spontaneous fission of ^{238}U is a rare event as the half-life is 10^7 longer than for alpha decay, it is much more destructive than alpha decay because it creates two heavy ions with high energy (~200 MeV).

Although strongly radioactive (average ThO_2: 8.79 wt %, average UO_2: 0.08 wt %, Van Emden et al. 1997), for poorly understood reasons, monazite does not become metamict (see transmission electron microscopy images in Black et al. 1984 and Seydoux-Guillaume 2002).

The X-ray patterns shown in Figure 3 was obtained on a 500 Ma monazite containing 13% Th and 0.25% U. It can be calculated that this monazite experienced about 7×10^{19} α/g. Meldrum et al. (1998) estimated that each α-decay in monazite produces 860 displacements. So this monazite should have suffered 3.7 displacements per atom, or one order of magnitude greater that the minimum dose necessary to make a mineral amorphous (Meldrum et al. 1997a). The crystalline integrity of this grain indicates that a mechanism must exist that is able to naturally restore monazite structure.

Recent work carried out to evaluate the role of monazite as a ceramic for nuclear waste storage suggest that the natural "radiation resistance" may be due to strong bonds between P and O and mineral structure, which has a lower symmetry compared to zircon, thereby mitigating α-particle damage (Krogstad and Walker 1994, Meldrum et al. 1996, 1997b). Thermal annealing appears to be an important mechanism to restore the damaged structure. For example, heavy ion irradiation experiments carried out at various temperatures demonstrate that it is not possible to amorphize a natural monazite grain above a critical temperature of 175°C (Meldrum et al. 1997b). For end-member $LaPO_4$,

the critical temperature is as low as 60°C. Karioris et al. (1981) determined that the recrystallization of a totally amorphous monazite was completed at 300°C. Electron irradiation is an efficient way to anneal metamict monazite, as total recrystallization is observed in a few minutes for 0.3 A/cm^2 using 200 kV electrons (Meldrum et al. 1997c). Therefore, ionization created by the alpha particles, or electrons from α decays in the U and Th chains, may partially anneal damage created by recoil nuclei.

Whatever the mechanism, monazite easily heals radiation damage and, thus behaves as a perfect structure in which all elements are bound together by chemical forces in a continuum. This is true for the parent (U, Th) and the final daughter product (Pb) as well as most intermediate decay products. Fluid phases cannot generally permeate through the structure and there are no amorphous domains from which leachable elements (Pb or U^{+6}) can easily escape (Davis and Krogh 2000).

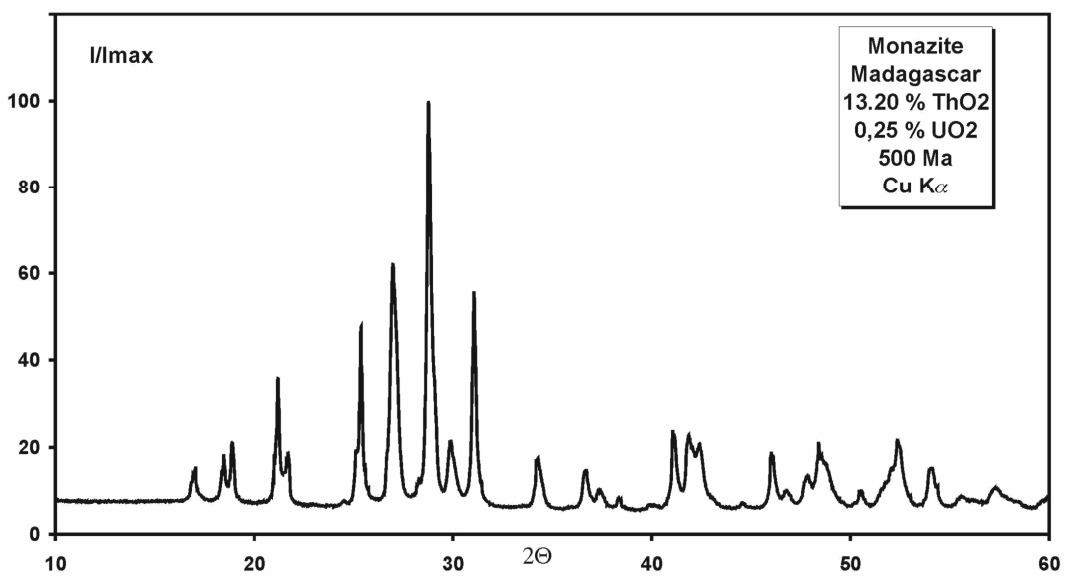

Figure 3. X-ray diffraction pattern of monazite.

Apatite

Mineral structure. The apatite structure is a complex association of a large Ca-site and PO_4 tetrahedra around a channel containing a big anion such as F, Cl, OH. In detail, the unit-cell has two types of Ca bearing sites: a seven-fold site, and a nine-fold site (see Boatner, this volume). The two sites are not equivalent, so large ions such as U and Pb are preferentially incorporated in the nine-fold site. Natural apatite contains mainly uranium as actinide element and almost no Th. The exact substitution mechanism is not fully understood. The replacement of Ca^{2+} by U^{4+} would require two charge compensation mechanisms. This can be achieved by complex substitutions such as $2\ Ca^{2+} + P^{5+} = U^{4+} + Na^{+} + Si^{4+}$, but numerous other possibilities exist as many ions are acceptable in the apatite structure. The U content of natural apatite thus remains limited and vacancies or defects could also play a role in this substitution. Pb is accepted in the apatite structure producing the end member phase pyromorphite. Unfortunately, this isostructural substitution may lead to high Pb^0 concentrations (Krogstad and Walker 1994). Thus, apatite, as with monazite, has little crystallographic tendency to behave as an open geochronometric system for U-Th-Pb.

Radiation effects. Radiation damage in apatite has been studied mainly for purposes of understanding the thermal behavior of fission tracks. Apatite is never found metamict, but this is surely in part due to its limited U-content. In rare cases, apatite can contain as

much U as zircon. Fission-track studies as shown than thermal annealing in apatite occurs at ~90°C over geologic time scales (Gleadow et al. 1983).

It has been recently demonstrated in apatite that α particle activity also heals recoil damage (Ouchani et al. 1997). While not demonstrated for monazite, both minerals are fundamentally constructed of PO_4 tetrahedra and thus this mechanism could also operate in monazite as well.

Xenotime

Mineral structure. Xenotime has a zircon-type structure combining eight-coordinated site containing Y and PO_4 tetrahedra. The Y site accepts ions with a smaller ionic radius than monazite. As a consequence, it is the structure preferred by $REEPO_4$ end-members from Tb to Lu, and YPO_4. A second consequence is that, contrary to monazite, xenotime favourably partitions U relative to Th, with mechanisms of substitution similar to monazite (Van Emden et al. 1997, Förster 1998b). Little is known about the incorporation of Pb in xenotime, but the large size of Pb and the preference of xenotime for smaller ions, suggests that it is unlikely that xenotime accepts Pb as easily as monazite.

Radiation effects. The radioactive element content of xenotime is lower than in monazite (e.g., Bea and Montero 1999) but still high enough to produce significant radiation damage. However, as with monazite, no metamict xenotime has ever been described. External irradiation experiments (Meldrum et al. 1997b) have shown that radiation damage in synthetic phosphates with xenotime structure are also healed easily at a temperature about 100°C higher than monazite. Thus the conclusions drawn above for monazite also likely apply to xenotime.

KINETIC PROPERTIES

Diffusion

Background. The phosphate minerals apatite, monazite and xenotime have strongly variable retention properties for Pb under crustal conditions. The mechanisms by which the daughter product can be lost include dissolution/reprecipitation reactions, recrystallization, and diffusive loss. The latter mechanism is likely a common source of discrepancy between a mineral date and the age of the rock from which it formed.

At sufficiently high temperature, daughter Pb will tend to migrate out of a crystal rapidly by diffusion. Since diffusion is strongly temperature dependent, transport rates rapidly decrease as temperature drops, eventually becoming negligible. In certain cases, the apparent age recorded by a mineral corresponds to the temperature at which the daughter product ceased to be lost from the crystal.

The Arrhenius relationship. Atoms diffusing through a crystalline solid are transferred via diffusion jumps between point defects in the crystal lattice. The formation of point defects result from one of two processes: intrinsic defects are thermally controlled defects which maintain electroneutrality, whereas extrinsic defects are caused by chemical impurities which create vacancies in order to conserve charge. Above absolute zero temperature, there is a finite probability of an atom having sufficient local thermal energy to jump from its current position to an adjacent defect. As temperature is raised, the probability of an atom in the Boltzmann distribution acquiring the threshold energy to make this jump increases exponentially. Thus the number of atoms jumping into adjacent vacancies is a function of both the fraction of vacant sites and the fraction of atoms having the necessary thermal energy to overcome the activation barrier. Because both the rate of defect formation and migration involve an exponential dependence, the diffusivity is given by the Arrhenius relationship,

$$D = D_o \exp(-E/RT) \quad (1)$$

where E is the activation energy, D_o is the frequency factor, R is the gas constant, and T is absolute temperature. Note that on a plot of 1log$D$ vs. 1/T (Fig. 4), the slope of the line is proportional to E and the y axis intercept is log(D_o).

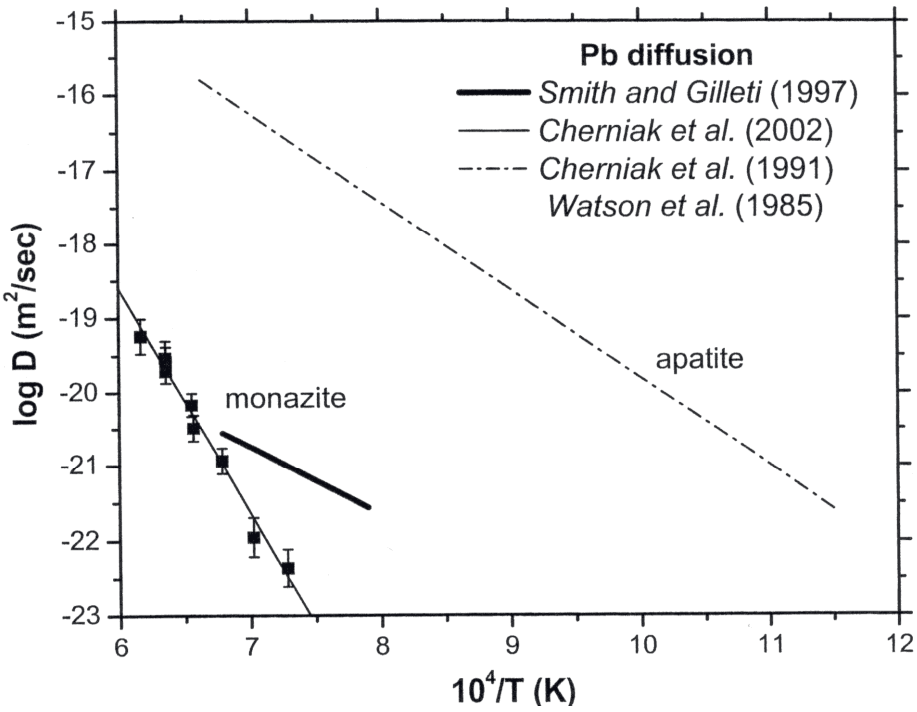

Figure 4. Arrhenius plot showing results of Pb diffusion experiments in monazite and apatite. The apatite data are combined from the studies of Watson et al. (1985) and Cherniak et al. (1991). There is a substantial discrepancy between the two Pb diffusion results for monazite that remains unexplained.

The diffusion equation. The general problem of unsteady-state diffusion within a solid involves the prediction of the concentration distribution C(x,y,z) within a solid as a function of the space coordinates and time, t. To derive an equation that can be solved for $C(x,y,z,t)$, conservation of mass and Fick's first law (i.e., the rate of transfer of mass per unit area is proportional to the concentration gradient, see Fick 1855) are applied to a differential control volume. The resulting expression is the diffusion equation

$$\frac{\partial C}{\partial t} = D\left(\frac{\partial^2 C}{\partial x^2} + \frac{\partial^2 C}{\partial y^2} + \frac{\partial^2 C}{\partial z^2}\right) \quad (2)$$

where D is the diffusion coefficient. Solutions of the diffusion equation can be obtained for a number of initial and boundary conditions covering simple concentration distributions and diffusion geometries (Crank 1975). These solutions have two distinct types: either an infinite trigonometric series or a solution involving the error function. In one dimension, x, the diffusion equation has the form

$$\frac{\partial C}{\partial t} = D\frac{\partial^2 C}{\partial x^2} \quad (3)$$

Using a coordinate transformation, Equation (3) can be modified to describe radial flow in a sphere (Crank 1975). The solution of this equation for the case of a sphere of radius r with an initially uniform concentration, C_o, held in an infinite reservoir of zero concentration can then be translated into terms of fractional loss by integrating the mass

loss occurring over the diffusion interval. This fractional loss, f, is given by

$$f = 1 - \frac{6}{\pi^2} \sum_{n=1}^{\infty} \frac{1}{n^2} \exp(-Dn^2\pi^2 t / r^2) \quad (4)$$

In the case of short diffusion times (i.e., only near surface penetration), it can be useful to approximate a mineral with a planar boundary as a semi-infinite medium. For the case of diffusion from a well-stirred semi-infinite reservoir at concentration C_o into a half space initially at zero concentration, the concentration distribution is given by

$$C = C_0 \operatorname{erfc} \frac{x}{\sqrt{4Dt}} \quad (5)$$

where x is the spatial position relative to the boundary at $x = 0$, t is the diffusion time, and erfc is the complimentary error function (erfc = 1 – erf z). Values of $x / \sqrt{4Dt}$ close to $^1/_2$ are essentially unmodified by the error function. Thus it is convenient to define the characteristic diffusion time necessary to change concentration at a specified position by half (i.e., $C/C_o = 0.5$) as $t = x^2/D$.

The closure equation. Minerals originating at deep crustal levels undergo a transition during slow cooling from temperatures that are sufficiently high that the daughter product escapes as fast as it is formed, to temperatures sufficiently low that diffusion is negligible and the retention of radiogenic isotopes by the mineral can be thought of as complete. Between these two states there is a continuous transition over which accumulation eventually balances loss, then exceeds it. The calculated age in this situation relates to the transition interval – the apparent age is the extrapolation of the total accumulation part of the curve to the time axis, which implicitly corresponds to an apparent temperature at which the bulk system became closed (Dodson 1973).

The exponential decay of daughter product loss with time, a consequence of the form of the Arrhenius equation, allows for a closed mathematical solution to the diffusion problem. Dodson (1973) derived a general solution of the accumulation–diffusion–cooling equation for a single diffusion length scale, r, using appropriate substitutions and variable boundary conditions that reduced the problem to an equation identical to Fick's second law. This equation is then be solved using general infinite series solutions (Carslaw and Jaeger 1959) for various geometries yielding expressions for the concentration distributions. Dodson (1973) then evaluated the coefficients, which reduce these expressions to a single characteristic value he called the closure temperature (T_c) which is given by

$$\frac{E}{RT_c} = \ln\left(\frac{ART_c^2 D_0 / r^2}{E\, dT / dt}\right) \quad (6)$$

where A is a geometric constant (sphere = 55, cylinder = 27, plane sheet = 8.7), and dT/dt is cooling rate.

Experimental determination of diffusion parameters. Although isotope exchange can be enhanced by fast-path diffusion along crystalline defects, mechanical grain size reduction, or structural decomposition, volume diffusion is the rate limiting transport mechanism in crystalline solids. In those cases where non-diffusional effects are inactive, thermal history information can be extracted from geological materials if the volume diffusion parameters are known. The approach is to perform diffusion experiments at temperature well above those of geological relevance and then extrapolate the results to lower temperatures using the systematic temperature dependence of the Arrhenius relationship (Eqn. 1). Note, however, that extension of these data may have no meaning if, for example, a diffusion mechanism with lower temperature dependence is encountered over the extrapolated portion. We first briefly review the requirements for the

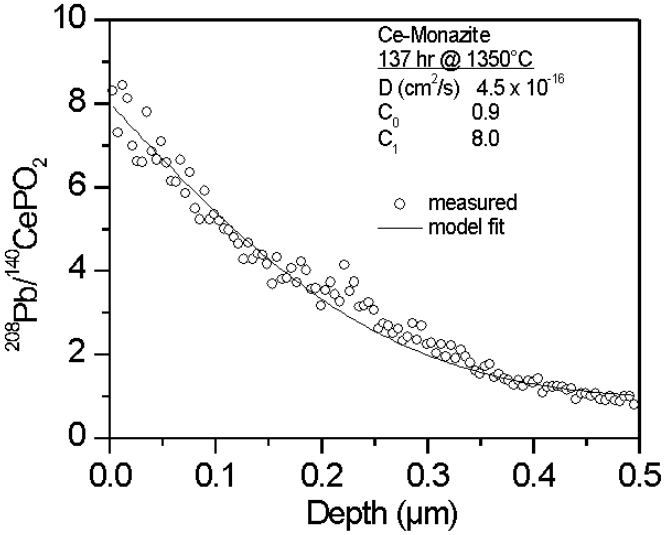

Figure 5. Characteristic form of an error function profile.

measurement of intercrystalline diffusion and summarize current knowledge of the diffusion of Pb in apatite and monazite.

The requirements of a diffusion study of a crystalline solid vary depending on the nature of the experiment, but two criteria must be met in all cases: the mineral must remain stable throughout the duration of the experiment and the initial distribution of the diffusing substance must be known. For purposes of interpretation, diffusion experiments should be designed to address questions regarding chemical vs. tracer diffusion or wet vs. dry conditions. If an isothermal experiment can be designed such that an effectively constant reservoir of diffusant is maintained on a planar surface of a mineral of known or zero concentration of the diffusing species, then knowledge of the concentration distribution (i.e., C as a function of x) can be translated into a value of D using Equation (5). The characteristic form of an error function profile (Fig. 5) can itself be used as a test of whether diffusion was the rate limiting transport mechanism during the experiment. Typically, analysis of these types of experiments is carried out with the ion microprobe using depth profiling mode, or with Rutherford backscattering (see Ryerson 1987).

Diffusion of Pb in monazite

Early geological estimates for the closure temperature of Pb in monazite range from 530°C (Black et al. 1984) to 600°C (Köppel et al. 1980). However, recent evidence suggests the U-Th-Pb system must remain closed to Pb loss through upper sillimanite zone conditions (Copeland et al. 1988, Smith and Barreiro 1990, Spear and Parrish 1996). A closure temperature of Pb in monazite was estimated by Copeland et al. (1988) at 720-750°C for 10-100 μm crystals cooled at 20°C/Ma, based on the presence of inherited monazite in a Himalayan leucogranite. Parrish (1990) suggested a closure temperature of 725±25°C on the basis of a preserved Pb loss profile in monazite from a paragneiss formed under upper amphibolite conditions. Suzuki et al. (1994) calculated closure temperatures for Pb diffusion in monazite as a function of grain size and cooling rate. For a 100 μm monazite, their results indicate closure temperatures of 650°C and 720°C, assuming respective cooling rates of 10 and 100°C/Myr.

In an early experimental study of sintered monazite, Shestakov (1969) estimated an activation energy of 60 kcal/mol by volatilizing Pb in a stream of nitrogen at temperatures between 800 and 1100°C. Smith and Giletti (1997) measured the tracer diffusion of Pb in natural monazites using ion microprobe depth-profiling and observed Arrhenius parameters of E = 43±11 kcal/mol and D_o = 6.6 × 10^{-15} m^2/sec in the temperature range of 1200 to 1000°C (Fig. 4). They found that transport parallel to the *c*-

axis is two to five times slower than perpendicular to c.

In a combined Rutherford backscattering and ion microprobe study, Cherniak et al. (2002) reported E = 149±9 kcal/mol and D_o = 0.94 m^2/sec for Pb diffusion in synthetic monazites in the temperature range 1150 to 1350°C (Fig. 4). This activation energy is over three times higher than the value reported by Smith and Giletti (1997), but diffusivities in the overlapping temperate range (i.e., between 1200 and 1150°C) were approximately the same. Subsequent studies utilizing natural monazites have confirmed this higher activation energy (Cherniak et al. 2002). The large discrepancy between the results of Smith and Giletti (1997) and Cherniak et al. (2000, 2002) is not fully understood, but analytical artifacts may play a role. In any case, the activation energy of Smith and Giletti (1997) is anomalously low.

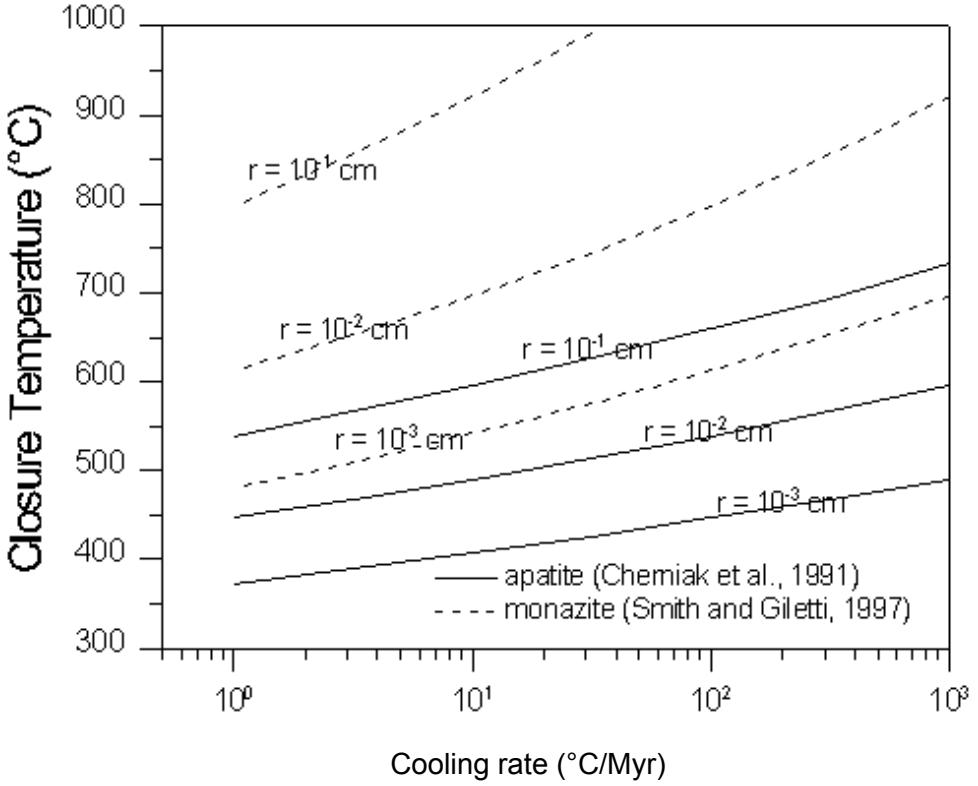

Figure 6. Closure temperature vs. cooling rate for apatite and monazite, assuming a spherical geometry with radius (r) indicated.

Using the diffusion data of Cherniak et al. (2000, 2002) and assuming spherical geometry, calculated T_c's for a range of cooling rates and diffusion domain sizes of 100 and 10 μm are shown in Figure 6. Assuming that the experimental study of Cherniak et al. (2000, 2002) is correct, the concept of closure is largely irrelevant to the U-Th-Pb monazite system under crustal conditions as Pb is predicted to be essentially immobile. Because disturbances to the U-Th-Pb system in monazite are widely reported (indeed, it was once believed that the T_c was <600°C, see Köppel et al. 1980, Black et al. 1984), mechanisms other than diffusive exchange (e.g., recrystallization, dissolution/reprecipitation) must be relatively common. Even prolonged thermal excursions at high crustal temperatures would have little effect on the U-Th-Pb monazite system. For example, a heating episode of 10-Myr duration at a temperature of 700°C would result in a diffusion profile with characteristic length-scale of only 0.25 μm (Eqn. 5).

Diffusion of Pb in apatite

Watson et al. (1985) used the electron microprobe to reveal gradients in Pb produced by annealing apatite in a dry environment in the temperature range 900 to 1250°C. The calculated Arrhenius parameters they obtained are: E = 70 kcal/mol and D_o = 350 m^2/sec. Subsequently, Cherniak et al. (1991) measured Pb diffusion in apatite in the broader temperature range 600 to 900°C using the significantly more sensitive Rutherford backscattering method and obtained results in good agreement with the data of Watson et al. (1985). The combined dataset yields an overall Arrhenius relationship of E = 54.6±1.7 kcal/mol and D_o = 1.2 m^2/sec.

Using the data of Cherniak et al. (1991) and assuming spherical geometry, calculated T_c's for a variety of cooling rates and diffusion domain sizes from 1000 to 10 μm are shown in Figure 6. For the case of a 100 μm diameter apatite, closure temperatures are in the range of 450 to 550°C for most geological relevant cooling rates. However, note that a heating episode of 1-Myr duration at a temperature of 600°C would cause a fractional Pb loss (Eqn. 4) of only 2.5% from an apatite of that size.

Diffusion of Pb in xenotime

In a Pb-isotopic transport and crystal chemical study of U-bearing minerals, Dahl (1997), suggests the closure temperature of Pb in xenotime is ≥ 750°C, similar to the results for monazite and epidote. Studies that date monazite and xenotime found in the same rock typically yield similar ages (e.g., Hawkins and Bowring 1997), suggesting that the minerals record similar closure temperatures or crystallization events. We speculate that the U-Pb system in xenotime is less retentive than monazite, as few examples of magmatic xenotime containing inherited U-Pb ages have been documented and the Y content in most magmatic rocks (which controls the solubility of xenotime) is about an order of magnitude less than LREE (which control monazite solubility), thus restitic xenotime from anatectic events may be rare. This idea may be invalid as Viskupic and Hodges (2001) report older ages preserved within both xenotime and monazite grains separated from a Himalayan orthogneiss. Clearly, obtaining more geochronologic data and experimental studies of the diffusion of Pb in xenotime are required to ascertain the significance of the mineral's age.

DATING APPROACHES

A variety of methods are currently being utilized to obtain U-Th-Pb ages of phosphates, including isotope dilution mass spectrometry, secondary ion mass spectrometry, chemical Pb dating, and laser ablation-inductively coupled plasma-mass spectrometry. We discuss these methodologies in turn and describe their relative merits in specific applications. Note that many recent studies consider combining the techniques described below as a means to maximize the benefits and circumvent drawbacks (e.g., Poitrasson et al. 1996, Cocherie et al. 1998, Crowley and Ghent 1999, Paquette et al. 1999, Poitrasson et al. 2000, White et al. 2001). Other recently developed techniques not presented here include proton microprobe analysis (e.g., Bruhn et al. 1999) and energy-dispersive, miniprobe, multielement analysis (Cheburkin et al. 1997).

Isotope dilution mass spectrometry

Mass spectrometers are fundamentally designed to determine isotope ratios. For example, the Pb isotopic composition of a U- and Th-bearing phosphate can be measured directly using a thermal ionization mass spectrometer provided the instrumental mass fractionation is known or can be assessed in the course of the analysis. Determining absolute abundances of isotopes requires a technique called isotope dilution in which a pre-determined quantity of a 'spike' of known but exotic isotope composition is added to

an aliquot of sample containing an unknown amount of the same element. Thus the isotopic composition of the mixture can be used to determine the amount of the element present in the unknown. In the case of elements containing more than one primordial isotope, instrumental mass fractionation can be addressed by correcting the measured isotopic composition of isotopes with a constant ratio in nature to the known value. Because Pb contains only one isotope that is neither radioactive or the product of radioactive decay (i.e., ^{204}Pb), isotope ratio precision is limited by the level of control on instrumental discrimination (typically ~1 ‰) unless a double spike (e.g., a mixture of ^{210}Pb and ^{205}Pb) is utilized. In the case of determining U and Th abundances, mixed spikes of ^{234}U and ^{230}Th, for example, can be used. Precision of inter-element ratios (i.e., ^{208}Pb/^{232}Th or ^{206}Pb/^{238}U) of ~0.2% are routinely achieved (e.g., Mattinson 1994).

High precision monazite, xenotime and apatite ages of single and multiple grains and fragments have been obtained using this approach (e.g., Krogstad and Walker 1994, Searle et al. 1997, Viskupic and Hodges 2001) and characterization of standard materials for other U-Th-Pb methods are generally based on isotope dilution measurements (e.g., Zhu et al. 1998, Sano et al. 1999a, Harrison et al. 1999a, Willigers et al. 2002). The high precision attainable by this approach has allowed the identification of important chronological characteristics of phosphate minerals such as the presence of an inherited component (e.g., Copeland et al. 1988) and unsupported daughter products from disequilibrium isotopes (e.g., Schärer 1984). These issues have the potential to limit the accuracy of data interpretations. If isotopic measurements are carried out using Faraday cup detectors, whole single grains, or more commonly aggregates of grains, are dissolved for analysis. This reliance on mineral separation can limit age interpretation textural relationships are destroyed, and unsupported Pb* from inclusions may be incorporated (Hawkins and Bowring 1997). In response to these concerns, less precise methods to date phosphate minerals have been developed that preserve textural relationships, and in some cases, the dated grain itself.

Secondary ion mass spectrometry

Spot analysis. Ion microprobe dating of monazite takes advantage of the kinetic energy distribution of U^+, Th^+, and Pb^+ ions sputtered from the grain using a primary oxygen (O^- or O_2^-) beam focused to a 10-20 μm diameter spot (Harrison et al. 1995, 1999a; Zhu et al. 1998, Stern and Sanborn 1998, Stern and Berman 2000, Petersson et al. 2001). At a mass resolving power of ~4500, all Pb and Th isotopes are resolved from any significant molecular interferences (Harrison et al. 1995). Zhu et al. (1998) report U and Pb peaks resolved in monazite at 6000, but operate with a mass resolving power of 2000 assuming interferences are negligible. However, an unidentified isobar at 203.960 amu complicates determination of $^{204}Pb^+$ in monazite with higher Th contents (Stern and Sanborn 1998, Stern and Berman 2000). In the case of Th-Pb dating, a linear relationship between $^{208}Pb^+/Th^+$ versus ThO_2^+/Th^+ is observed for monazite grains with a known uniform Pb/Th ratio (Harrison et al. 1995, 1999a; Catlos et al. 2002b). Isotopic data collected from several ion microprobe spots on the age standard define this linear relationship and allow a correction factor to be derived by dividing the measured $^{208}Pb^+/Th^+$ of a standard grain at a reference ThO_2^+/Th^+ value by its known daughter-to-parent ratio. This correction factor permits the determination of Pb/Th ratios of unknown grains measured under the same instrumental conditions. Precision is generally limited by the reproducibility of the calibration curve, which is typically ±2%. Stern and Berman (2000) report similar uncertainties for U-Th-Pb ion microprobe measurements. Rather than assessing the relative inter-element sensitivity, DeWolf et al. (1993) used an ion microprobe obtain ^{207}Pb/^{206}Pb spot ages on Precambrian monazites.

Ion microprobe analysis of apatite is outlined by Sano et al. (1999a), whereas

xenotime ion microprobe dating is described by Petersson et al. (2001). A mass resolving power of 4500 is used to resolve U and Pb peaks in xenotime (Petersson et al. 2001) and 5800 in apatite (Sano et al. 1999b).

For single-grain spot analysis, mineral grains are typically mounted in epoxy, polished, and photographed in reflected and transmitted light (e.g., Stern and Berman 2000). Backscattered electron (BSE) images are taken of individual grains to record zoning patterns and the probe spot can be focused on selected sites within the mineral grain (e.g., Zhu et al. 1997, Ayers et al. 1999, Sano et al. 1999a, Zhu and O'Nions 1999a). The spatial resolution of the ion microprobe can be <10 μm and the crater depth is generally <2 μm during a typical 15-minute analysis. However, misleading results are possible if the beam overlaps areas of substantially different age. Detailed images of the grain may help to resolve this issue if a correlation exists between chemical composition and age (see Zhu and O'Nions 1999b).

Petersson et al. (2001) note that matrix effects limit the accuracy of the xenotime ion microprobe ages and they were unable to precisely reproduce the U-Pb ages of their standards. For example, xenotime standard 88102-5 has a concordant ^{238}U-^{206}Pb age of 919±5 Ma, whereas ion microprobe analyses yielded 934±4 Ma. Zhu et al. (1998) explores potential matrix effects during monazite ion microprobe analysis, but analytical methods outlined in their paper preclude conclusive interpretations. Stern and Sanborn (1998) report that the use of high-Th monazite standards may lead to errors in measuring ages of low-Th grains, and suggest the use of compositionally matched standards and unknowns.

Depth profiling. In the 'classical' approach to U-Pb dating (e.g., Compston et al. 1984), the spatial resolution of a measurement is defined by the diameter of the primary ion beam spot. Given the trace concentration levels of Pb expected, even in monazite, and reasonable analysis times, typical probe spot diameters of ca. 10 μm are often required. However, because virtually all secondary ions originate from the first or second atomic layer of the instantaneous sample surface, atomic mixing due to the impacting primary ions and geometric effects on crater production are the essential limiting factors on depth resolution. The resulting spatial resolution offered by depth profiling is potentially two orders of magnitude higher than spot analyses. Care must be taken in this analysis mode to ensure material sputtered from the crater walls is not analyzed. This can be accomplished by placing an aperture in front of the emergent ion beam that restricts entry into the mass spectrometer to only those ions originating on the crater floor.

Grove and Harrison (1999) investigated the feasibility of obtaining Th-Pb age profiles in the surface regions of natural monazites and found that ion intensities were adequate to resolve age differences of <1 Myr with better than 500 Å depth resolution in late Tertiary monazites. These age gradients were then used to extract continuous thermal history information from which they constrained the displacement history of a Himalayan thrust. The sputtering of natural surfaces was found to yield inter-element calibration plots of similar reproducibility to that of polished surfaces.

In situ *ion microprobe dating.* Numerous studies report U-Pb or Th-Pb ages of phosphate minerals grains in thin section (= *in situ*) using the ion microprobe (DeWolf et al. 1993, Harrison et al. 1997a, Zhu et al. 1997, Catlos 2000, Foster et al. 2000, Catlos et al. 2001, 2002a; England et al. 2001, Gilley 2001, Petersson et al. 2001, Robinson et al. 2001, Gilley et al. 2002). The spatial resolution allows preservation of textural relationships, and thus potentially less ambiguous age interpretation.

Monazite is an ideal mineral for *in situ* geochronology as it appears in pelitic lithologies at conditions ranging from the garnet to the aluminosilicate isograds (e.g.,

Smith and Barreiro 1990, Harrison et al. 1997a, Bingen and Van Bremen 1998, Ferry 2000, Wing et al. 2002) and inclusions in garnet appear armored against daughter product loss (e.g., Montel et al. 2000). Garnet-bearing assemblages allow the determination of pressure-temperature (P-T) conditions (e.g., Spear 1993), and when combined with monazite age data, suggest a powerful combination for ascertaining the evolution of metamorphic terranes (DeWolf et al. 1993, Harrison et al. 1997a, 1998; Foster et al. 2000, Terry et al. 2000, Catlos et al. 2001, Gilley 2001). Individual grains are ordinarily identified and characterized texturally and chemically by using the electron microprobe, then either cut out with a high-precision saw, or drilled out with a diamond drill corer. The fragments are cleaned and mounted in epoxy with a pre-polished block of age standards. Zhu et al. (1997) and Catlos et al. (2002b) briefly outline methods of *in situ* monazite chronometry, whereas Petersson et al. (2001) describe methods for obtaining *in situ* ion microprobe xenotime ages.

Chemical Pb dating

Background. The concept of chemical U-Th-Pb dating emerged shortly after the discovery of radioactivity (e.g., Holmes 1911). As U and Th disintegrate ultimately to Pb, it is possible to estimate an age solely from the elemental proportion of Pb, U and Th. This age has geological meaning only if two conditions are met: (1) all Pb is radiogenic, or at least, that the Pb° can be neglected, and (2) the system remained closed. The first condition is only approximated in minerals rich in U and Th and poor in Pb, such as zircon, monazite, thorite, uraninite, thorianite, and xenotime, whereas the second condition cannot be tested independently without isotopic data. Because isotopic dating is now so efficient, chemical dating is now generally restricted to *in situ* dating techniques.

If a mineral is sufficiently old and rich in Th and U, Pb* concentrations can be high enough to be detectable using an electron microprobe. Analysis of all three elements then provides an estimate of age. This method has been widely used in uranium-ore studies, as pitchblende produces high Pb* contents in relatively short times. Recently this technique has been applied with success to monazite (Suzuki and Adachi 1991, 1994; Montel et al. 1994, 1996; Williams and Jercinovic 2002), and, with more difficulty, to zircon, and xenotime (Suzuki and Adachi 1991, Geisler and Schleicher 2000)

The electron microprobe's detection limit for Pb can be a limitation in the precision of the chemical age results (e.g., Olsen and Livi 1998) as can potentially the assumption that monazite is "generally concordant" (e.g., Cocherie et al. 1998) and does not incorporate "appreciable amounts" of Pb° during growth (e.g., Scherrer et al. 2000). Finger and Helmy (1998) suggest that monazite is "resistant to post-crystallization disturbance and mostly free from inheritance." These assumptions are not always met as numerous studies indicate that the mineral can accumulate excess ^{206}Pb (Schärer 1984, Parrish 1990, Schärer et al. 1990, see also Fig. 2), Pb° (e.g., Coleman 1998, Catlos et al. 2001, 2002a; see also Table 3), contain inherited Pb* (Copeland et al. 1988) and sustain Pb loss (Catlos et al. 2001).

The attraction of electron microprobe monazite dating is that this apparatus is widely distributed and accessible to most geologists. Modern microprobes are highly automated, are easy to handle, have expanded mapping and profiling capacities, and have excellent electronic and optical visualizing devices. For example, electron microprobe maps showing the distribution of ages within single grains have been reported by several workers (Braun et al. 1998, Cocherie et al. 1998, Crowley and Ghent 1999, Williams et al. 1999, Williams and Jercinovic 2002). Cocherie et al. (1998) suggests electron microprobe dating has "no competitor for dating complex polygenetic monazite, especially when two events are recorded." Cocherie et al. (1998) warrant that the spatial resolution of the electron microprobe (1-5 μm) is ideal for measuring ages of regions

Table 3. Summary of U-Pb analytical data from two mineral separation/isotope dilution case studies.[a]

Sample[b]	*Description*	N[c]	*$^{206}Pb/^{238}U$ age (Ma), ±1σ*	*$^{207}Pb/^{235}U$ age (Ma), ±1σ*	*%^{206}Pb*[dd]*
AS-31 Leucogranite orthogneiss					
MA		3	*36.7 (0.2)*	36.4 (0.2)	99.1
MB		9	34.4 (0.1)	33.7 (0.1)	99.1
MC	*visible core*	1	36.4 (0.1)	35.9 (0.1)	98.6
MD		1	37.2 (0.1)	36.2 (0.1)	99.1
			36.2 (0.1)144[e]	35.6 (0.1)138	
AS-38 Deformed migmatitic leucosome, unit 1					
MA		>50	32.5 (0.1)	33.5 (0.1)	92.8
MB		4	23.3 (0.1)	23.3 (0.1)	98.1
MC		15	35.8 (0.1)	35.8 (0.1)	98.4
MD		7	34.8 (0.1)	34.8 (0.1)	98.4
			31.6 (0.1)3253	31.9 (0.1)3338	
AS-23 Deformed migmatitic leucosome, unit 1					
M1		1	31.8 (0.1)	31.6 (0.1)	98.6
M3		1	29.9 (0.1)	29.7 (0.2)	98.0
M4	round	2	28.3 (0.3)	28.0 (0.8)	96.0
M5		2	29.5 (0.1)	29.2 (0.4)	97.5
M6		5	29.8 (0.1)	29.6 (0.2)	96.7
			29.9 (0.2)104	29.6 (0.4)99	
MCT-1 migmatitic pelitic schist					
Ma	clear, incls	1	20.9 (0.9)	20.7 (0.9)	99.1
Mb	clear, incls	1	21.5 (2.0)	*21.4 (2.0)*	98.6
Mc	clear, incls	1	18.3 (1.8)	18.2 (1.8)	98.1
Md	clear, incls	3	21.5 (1.2)	21.7 (1.2)	99.0
Me	clear, incls	5	20.6 (0.8)	20.5 (0.8)	99.2
Mf	clear, incls	15	28.0 (0.9)	30.5 (0.9)	99.2
Mg	clear, incls	20	23.8 (1.0)	24.7 (1.1)	98.8
			22.1 (1.3)9	22.5 (1.3)17	
MCT-93-88 foliated leucogranite					
M2a	clear	9	28.8 (1.8)	28.0 (1.7)	99.0
M2b	clear, incls	4	28.6 (9.4)	28.3 (9.3)	96.5
M2c	clear, incls	5	28.8 (3.1)	28.0 (3.1)	97.3
M2d	clear, incls	1	34.3 (1.4)	33.9 (1.4)	99.6
			30.1 (5.1)3	29.6 (5.0) 4	
DK-1 undeformed leucogranite					
Mf	clear	5	*19.3 (2.0)*	18.7 (1.9)	97.5
Mg	clear	4	19.4 (2.4)	19.0 (2.4)	97.1
Mh	clear	5	19.3 (2.5)	18.9 (2.4)	97.0
			19.3 (2.3)<1	18.9 (2.3)<1	
DK-2 undeformed leucogranite					
Mi	incls	>50	19 (73)	17 (67)	61.7
Mj	incls	>50	19 (70)	17 (64)	64.7
			19 (72)<1	17 (66)<1	

a. "AS" data from Hodges et al. (1996), whereas "MCT" and "DK" data from Coleman (1998). See Figure 2 for a concordia diagram of this and other Himalayan monazite data.
b. Sample name is followed by a description of the mineral grains if provided. "incls", inclusions.
c. Number of grains analyzed.
d. % radiogenic ^{206}Pb, calculated using $^{206}Pb/^{204}Pb$ of 18.7 (Stacey and Kramers 1975). Note that a majority of monazite grains have high (>95%) Pb* contents.
e. Average age, Ma (±1σ) and Mean Square Weighted Deviation calculated using 1σ errors. The majority of data reported from single samples are inconsistent with a single population.

within monazite grains inaccessible to conventional U-Pb dating techniques and too small for the ion microprobe analysis. This view appears to be based on a misunderstanding of the inherent spatial resolution of the ion microprobe which can be as low as a few μm's in spot analysis mode or as much as two orders of magnitude lower in depth profiling mode (e.g., Harrison et al. 1997b, Grove and Harrison 1999).

The inability of electron microprobe to provide isotopic ratios is a potentially serious limitation of this technique. However the open/closed system problem can be, in part, assessed by comparing ages to chemical compositions (e.g., Suzuki et al. 1994, Braun et al. 1998). Finally we should note that the electron microprobe is a non-destructive method and thus can be combined with other techniques. For example, electron microprobe analyses in a thin section analyzed afterward by ion microprobe or grains mounted in epoxy, extracted and dated by thermal ionization mass spectrometry.

Technical and analytical basis for electron microprobe dating. Electron microprobe dating requires precise analyses of U, Th, and Pb. For these heavy elements, M-lines are used which are intrinsically weak and broad. Special attention must be paid to the Pb analyses because the precision and accuracy on this element directly controls the precision and accuracy of the calculated age. Refer to the original papers to find details of the analytical conditions (Suzuki and Adachi 1991, 1994; Montel et al. 1994, 1996; Rhede et al. 1996, Cocherie et al. 1998, Finger et al. 1998, Olsen and Livi 1998, Crowley and Ghent 1999, Williams et al. 1999, Scherrer et al. 2000).

As for any high-precision analysis with the electron microprobe, long counting times and high sample currents are necessary. Typical counting times are several minutes, especially on the Pb peaks and backgrounds. Typical probe currents range from 50 to 150 nA. The accelerating voltage used varies from 15 kV to 40 kV. When M lines are utilized, low accelerating voltage (15 kV) can be used. With such a low voltage, the excited domain is less than 2 μm in diameter, and matrix corrections are limited.

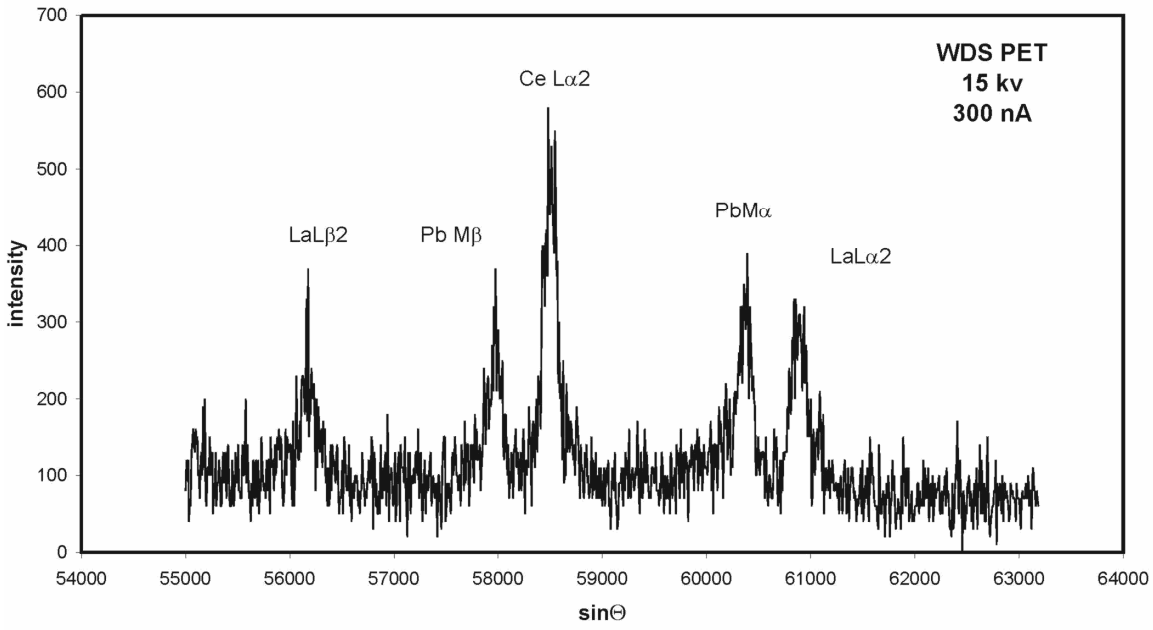

Figure 7. Wavelength dispersive spectrometry (WDS) scan of the region corresponding to the two M-lines for Pb. Additional interference that are not readily visible are the two Th-Mζ_1 and Th-Mζ_2 line around the Pb-Mα line and the Y-Lα line at the Pb-Mα position. The subscript 2 is for second-order lines.

The choice of lines and background positions are key to the procedure (Fig. 7). There is no general agreement on the best lines and the corresponding background positions, because, for each microprobe, as a function of analytical condition, the optimal positions are different and must be empirically determined by the user. The main difficulties arise from the presence of other X-rays lines interfering with peaks or background positions (Th M_β on U M_α, K K_α on U M_β, Y L_α and Th M_ζ on Pb M_α second order Ce L_α on Pb M_β). This require careful investigations of the Wavelength Dispersive Spectrometry (WDS) signal of monazite around the M-lines for Pb, U, Th. The theoretical WDS spectrum presented in Scherrer et al. (2000) should be used only as a general guide because the actual spectrum may differ significantly from those calculated ones. As an example, we report in Figure 7 the WDS diagram around the Pb lines for a monazite containing about 1% Pb, at 300 nA and 15 kV, on a Cameca SX-50 microprobe. [See Chapter 8 by Pyle et al., this volume, for additional information on microprobe analysis of phosphates.]

Data processing. The raw peaks and background data are processed through ZAF, PAP, or equivalent matrix correction programs. There are no particular difficulties at this stage but care must be taken to analyse the light elements of monazites (Ca, Y, Si, P), because they significantly influence matrix correction coefficients. A variety of standards are used for UO_2, ThO_2, and multiple compounds for Pb, including synthetic glass, PbS, and vanadinite. Errors in U, Th, and Pb contents, as well as detection limits are obtained by classical methods, the best being the mathematical analysis of Ancey et al. (1978). Detection limits can be as low as ±80 ppm on Pb, with use of long counting times, high probe currents, and a modern instrument.

The amount of Pb in a monazite of age τ is calculated from:

$$Pb/M_{Pb} = Pb^0 + Th/232 \cdot (e^{(\lambda_{232} \cdot \tau)} - 1) + U/235 \cdot (1 - R) \cdot (e^{(\lambda_{235} \cdot \tau)} - 1) + U/238 \cdot R \cdot e^{(\lambda_{238} \cdot \tau)} - 1 \quad (7)$$

where M_{Pb} is the molar weight of Pb, and 232, 235, 238 are the molar weights of ^{232}Th and ^{235}U and ^{238}U, respectively. Decay constants are represented by λ_{232}, λ_{235}, λ_{238} and R is the $^{238}U/^{235}U$ atomic ratio (137.88). Because Pb in monazite is primarily ^{208}Pb, we can assume 208 to be the molar weight of Pb. Equation (7) must be solved iteratively for τ. Age uncertainty depends on the uncertainty on Pb, Th, and U contents and is calculated by classical error propagation techniques, or by Monte-Carlo simulation. A property of the error in electron microprobe analysis is that the absolute error is almost constant for given analytical conditions (Ancey et al. 1978), thus relative errors are lower for higher Pb contents. As a consequence, absolute age errors are lower for higher U and Th contents.

A population of 10 to 50 ages is quickly and easily obtained from monazites using *in situ* electron microprobe dating techniques. Several statistical procedures for extracting as much information from this population as possible have been suggested. For example, the 0-dimension method (Montel et al. 1996) directly uses Equation (7), assuming Pb° can be neglected. Then each U, Th, Pb triad is transformed into an age with associated error. The statistical procedure is carried out on the age population with the goal of assessing two questions: (1) does the population represent a single geological event? and (2) what is the best estimate (with associated errors) for the age of this event? The answer to the second question is given by classical statistical formulae and the answer to the first by a statistical test. If the answer to the first question is no, another hypothesis must be developed. Montel et al. (1996) describe a procedure when two ages (or more) are suspected. The best representation of this method of calculation is the weighted-histogram representation that plots the probability as a function of age for the whole population (Fig. 8).

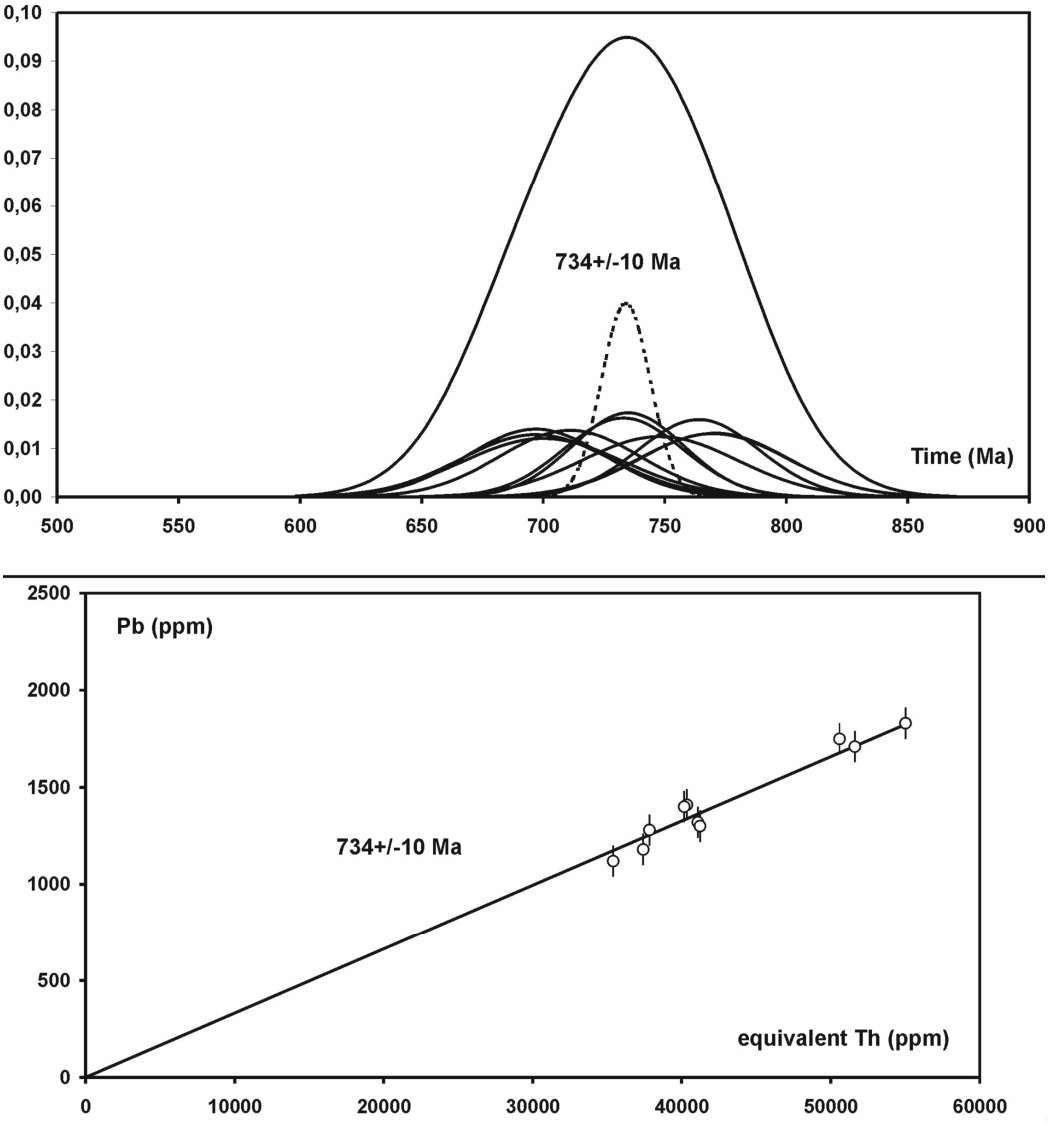

Figure 8. (Upper) weighted-histogram and (lower) isochron representation of a sample in which a single population of ages can be distinguished. The sample is a migmatite from Madagascar.

Suzuki and Adachi (1991, 1994) use a 1-dimension procedure in which Equation (7) is transformed into the equation of a straight line. They assume that Pb^0 is constant, and transform U content into a "fictive Th" content (i.e., the amount of Th that would give the same amount Pb than U for a given age). The sum of the real Th and fictive Th is an "equivalent Th" value, Th*. Plotting Pb versus Th* should give a straight line, the slope of which yields the age and the intercept at zero Th giving Pb^0. The advantage of this procedure is that it visually shows the entire population. However this procedure assumes that all grains have a unique Pb^0 content. A variant of this technique is to use the same representation, but to force the line through the origin. This should give the same age than the 0-dimension model, but provides an isochron-like representation. Two examples are reported in Figures 8 and 9. In both cases the weighted-histogram and the isochron-like representations are given.

Rhede et al. (1996) proposes a 2-dimensional procedure. However, Equation (7) can be considered a plane in Pb-Th-U space. If the ages given by Th-Pb system and U-Pb

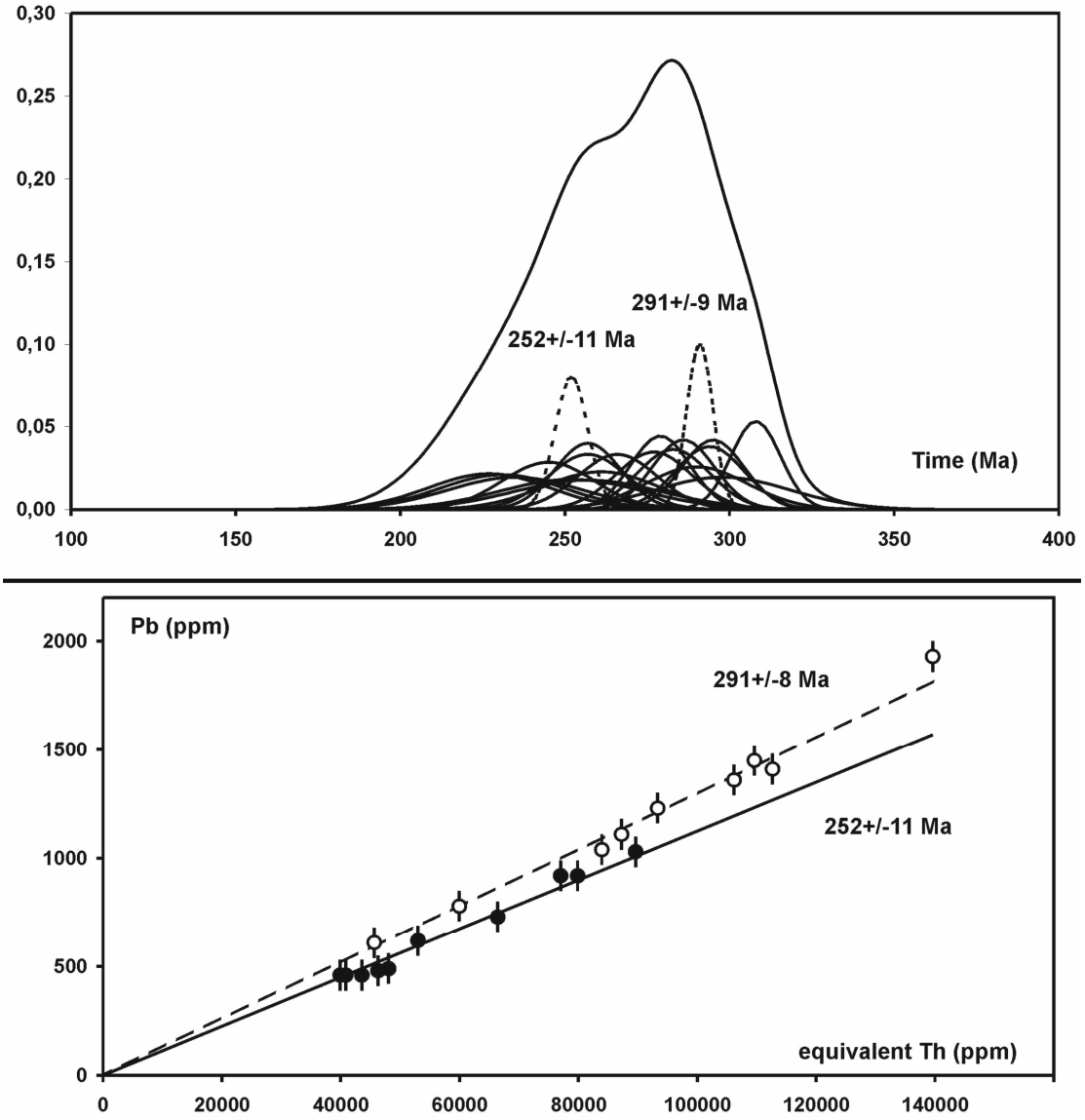

Figure 9. Upper—weighted-histogram. Lower—isochron representation of a sample in which two populations can be distinguished. The sample is a microgranite affected by a hydrothermal event. The older age is thought to be the magmatic age; the younger age may be the age of the hydrothermal event.

system are different, the best-fit plane in the Pb-Th-U space gives the two ages and Pb^0. The advantage of this method is to provide an estimate of system concordance by comparing the ages from derived from two different systems. However, this technique requires complex graphical representation and is more difficult to compute than the 0- or 1-dimensional methods. A modification proposed by Cocherie and Albarède (2001) considers the ratios Pb/U and Pb/Th instead of a Th-U-Pb diagram.

Whatever procedure used, a significant reduction of the error on ages is obtained when the whole data population is considered. With modern microprobes, statistically-reduced errors of ±10 Ma are commonly obtained; a value close to the maximum precision attainable as uncertainties related to matrix effect corrections, line interferences, Pb atomic weight, or standard composition, cannot be eliminated without changing analytical procedures.

Sample preparation. Two main types of samples have been used for monazite electron microprobe dating, both having advantages. The most direct method is to use uncovered rock thin sections prepared for electron microscopy. The advantages here are obvious: no specific preparation is required, and more importantly, the position of each dated grain in the thin section is known, and it is then possible to correlate the ages with the petrology of the sample. This is the preferred method when a complex history is anticipated in a sample. The best method to find monazite in thin section is electron imaging in BSE mode as monazite grains appear as bright grains (Scherrer et al. 2000). The exact nature of the grains must be confirmed by qualitative analyses using an energy dispersive system, or, on microprobe, by looking for high Th, Ce and P contents.

Another technique is to use separated grains mounted in epoxy resin. With this technique a great number of crystals can be analysed. However, small grains can be lost and the position of the grain in the rock is unknown, making the interpretation of the results difficult if the age population is mixed. This method however can be easily combined with a thermal ionization mass spectrometry dating study, for which monazite separation is always necessary.

Laser ablation-inductively coupled plasma-mass spectrometry

The lower precision results produced by *in situ* ion or electron microprobe dating of phosphate minerals compared to isotope dilution methods continue to impel development of alternative *in situ* approaches with the potential for high precision. Recently, laser ablation-inductively coupled plasma-mass spectrometry has been applied to monazite and apatite dating (Machado and Gauthier 1996, Poitrasson et al. 1996, 2000; Engi et al. 2001, Kosler et al. 2001, Willigers et al. 2002). With this method, a laser beam directly samples a selected portion of a mineral and ionized material is transferred into a mass spectrometer (see Willigers et al. 2002). The method excavates the mineral of interest with a laser spot size of 25-100 μm, making the technique applicable for *in situ* studies of phosphate minerals with larger grain sizes (Machado and Gauthier 1996, Willigers et al. 2002). Kosler et al. (2001) report U-Th-Pb monazite ages that are as young as several tens of million years with a precision better than 2%, whereas Willigers et al. (2002) reports apatite and monazite ages with uncertainties comparable to those determined by isotope dilution. These recent results contrast to the low precision reported by Machado and Gauthier (1996) testifying to the rapid development of this technique. Areas of continued development (see Willigers et al. 2002) include improvements to sensitivity, ion transmission, and laser methodology, which may lead to laser-ablation inductively-coupled plasma mass spectrometry becoming competitive for *in situ* U-Th-Pb dating with the spatial selectivity of the ion and electron microprobes.

U-TH-PB DATING OF MONAZITE

Prograde thermochronometry

In contrast to thermochronologic systems involving an isotopic closure transition, the use of prograde thermochronometers, such as U-Th-Pb monazite-in-garnet dating, permits mineral growth ages to be directly determined. Detrital monazite is unstable in most pelitic rocks at low grades (chlorite to biotite grades) as allanite or REE oxides appear to host REE and radiogenic isotopes (Smith and Barriero 1990, Kingsbury et al. 1993). Note that Rasmussen et al. (2001) reports ion microprobe U-Pb ages of monazite found in northern Australian Pine Creek shales, but the scarcity of the mineral in most low-grade metamorphic terranes preclude widespread application. In some pelitic rocks, neoformed monazite reappears at about the aluminosilicate isograd (Ferry 2000, Wing et al. 2002). Thus, U-Th-Pb dating of monazite potentially times aluminosilicate growth and formation of a metamorphic isograd. Transects along the Himalayan inverted meta-

morphic sequences show allanite as the dominant mineral at lower metamorphic grades, whereas monazite appears coincident with garnet, suggesting that in this case, monazite ages can time garnet growth (Harrison et al. 1997a, Foster et al. 2000, Catlos et al. 2001, Kohn et al. 2001). In each case, major phase compositions can yield the thermobarometric conditions of formation (Spear 1993), and suggest the utility of monazite as a geochronometer in metamorphic terranes.

While the diffusive transport of Pb in monazite is slow under most crustal conditions (Smith and Giletti 1997, Cherniak et al. 2000, 2002), in certain cases it appears that monazite inclusions in garnet are armored against Pb loss (Montel et al. 2000, Catlos et al. 2001). Exploration of monazite growth prior to garnet growth can be addressed through phase equilibria (e.g., Pyle and Spear 1999) and trace element studies (e.g., Foster et al. 2000). For example, because Y and heavy REE are preferentially concentrated in garnet, their concentrations in monazite have been used to assess paragenesis, although Catlos et al. (2002b) found no correlation between composition and age.

A major complication facing *in situ* monazite analysis is the interpretation age data inconsistent with a single population (see Fig. 10). To address this issue, monazite chemical variability has been speculated to reflect timing information (e.g., Ayers et al. 1999, Zhu and O'Nions 1999a,b). For example, Foster et al. (2000) surmises that lower Y

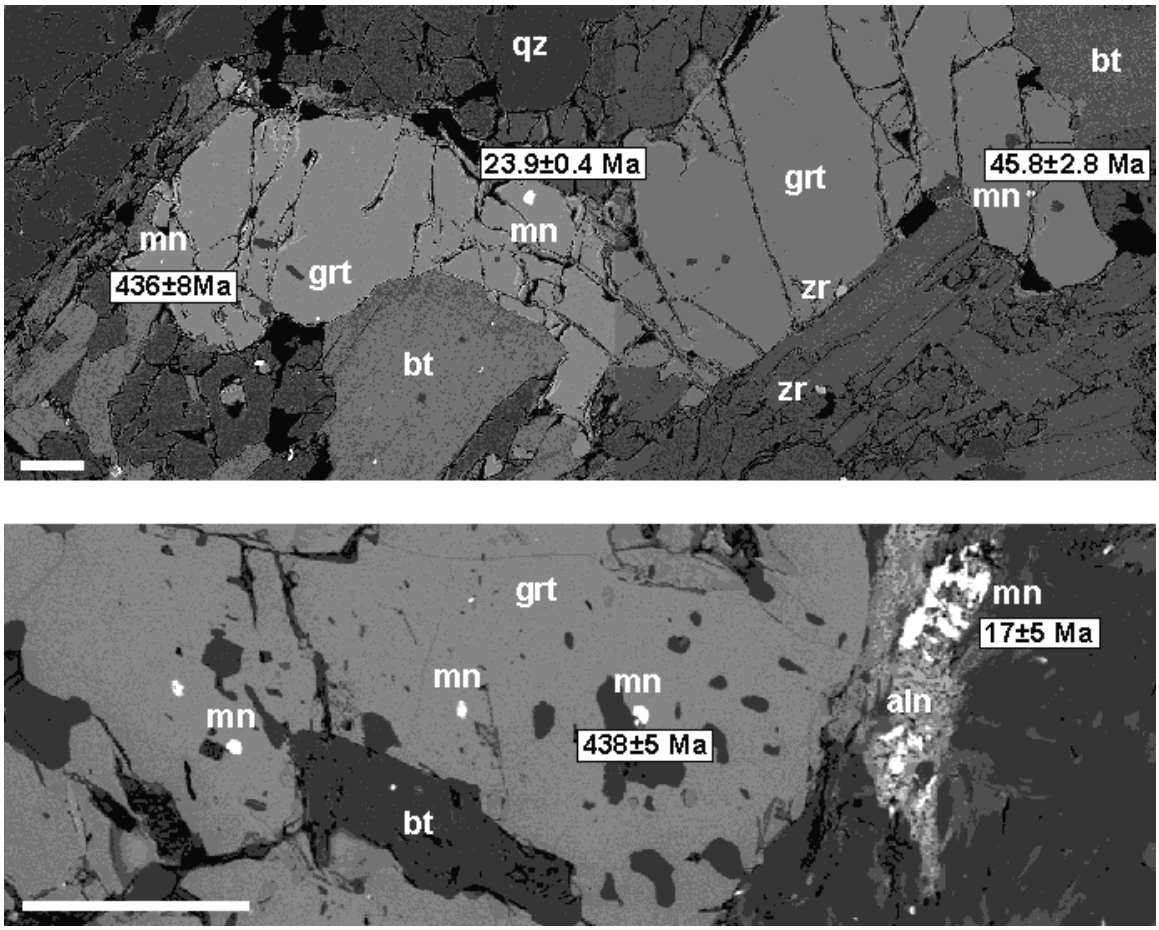

Figure 10. Backscattered electron images of (upper) Nepal Himalaya (Catlos et al. 2002a) and (lower) Turkey Menderes Massif samples. Monazite grains (mn) are seen as bright grains with ion microprobe Th-Pb ages are in boxes with 1σ errors. Other abbreviations include: grt, garnet; zr, zircon; bt, biotite; qz, quartz; aln, allanite. These samples were collected from regions that experienced complicated polymetamorphic histories, and they illustrate the benefit of an *in situ* technique for monazite geochronology.

concentrations in matrix monazites are clear evidence that the matrix grains crystallized at a later time than those included in the garnet (see also Bea and Montero 1999). Finger and Helmy (1998) suggest that monazite grains with higher Y contents at the rims indicate crystal growth under prograde temperature conditions. Zhu and O'Nions (1999b) found significantly lower amounts of Y and heavy REE in monazite grains in rocks containing garnet as a major mineral compared to grains found in samples without garnet and those speculated to form after garnet breakdown. However, Catlos et al. (2002b) report that monazite grains from several localities in Nepal and Vietnam, dated using the ion microprobe and chemically analyzed with the electron microprobe, show no correlation between LREE and Y composition and age. For example, an eastern Nepal sample contains ~500 Ma, ~45 Ma, and ~20 Ma monazite grains, consistent the timing of Pan-African and polymetamorphic Himalayan events (Fig. 10). The ~20 Ma grains contain 0.71-1.33 wt % Y_2O_3, ~45 Ma grains have 0.97-3.36 wt %, and a ~500 Ma grain has ~1.2 wt %. Instead of relying on monazite chemical composition, possibly influenced by bulk rock composition, reactions with other accessory minerals, crystal orientation, and the monazite-forming reactant (e.g., allanite), Catlos et al. (2002b) suggest garnet zoning patterns and peak P-T conditions facilitate age interpretation. Five sources of uncertainty explain complicated age distributions from monazite grains dated *in situ*: (1) Pb loss due to prolonged experienced above the closure temperature, (2) dissolution/reprecipitation along the retrograde path, (3) analytical uncertainties, (4) analyses of overlapping age domains, and (5) episodic monazite growth. Thermobarometric data and textural observations can assess potential polymetamorphism, retrogression, and in conjunction with diffusion studies, the predicted extent of monazite Pb loss.

Case studies

Isotope dilution. The Himalayan range has largely provided the backdrop for the development and understanding of the U-Th-Pb system in monazite. A large number of studies employ isotope dilution techniques to the analysis of separates of Himalayan monazites (e.g., Schärer 1984, Copeland et al. 1988, Parrish and Tirrul 1989, Nazarchuk 1993, Hodges et al. 1996, Parrish and Hodges 1996, Searle et al. 1997, Coleman 1998, Simpson et al. 2000). Many of these studies have addressed the temporal evolution of the Greater Himalayan Crystallines and High Himalayan leucogranites, rocks found in the hanging wall of the Main Central Thrust, a large-scale structure that largely created the Himalayan range (e.g., Harrison et al. 1999b). The Greater Himalayan Crystallines are speculated to have experienced a complicated metamorphic evolution (see Pêcher and Le Fort 1986). A first stage (Eocene-Oligocene) of Barrovian-type metamorphism, termed the Eohimalayan event, corresponds to burial of the nappe beneath the southern edge of Tibet (Le Fort 1996). During this stage the base reached 650-700°C and ~0.8 GPa. During a second stage (Miocene), termed the Neohimalayan event, the base experienced 550-600°C conditions, whereas the top records lower pressures and/or temperatures. The Neohimalaya has been associated with slip along the Main Central Thrust and the development of the High Himalayan leucogranites exposed at upper structural levels of the Greater Himalayan Crystallines (e.g., Harrison et al. 1997b).

High precision can be obtained from the isotope dilution approach, but the relative youth and low U contents of the Himalayan monazites often result in discordant ages with large uncertainties (see Nazarchuk 1993, Hodges et al. 1996, Coleman 1998). For example Table 3 summarizes several isotope dilution ages of aliquots of Himalayan monazite grains. Many ages are highly precise but inconsistent with a single population (e.g., samples AS-31, AS-38, AS-23). The number of grains analyzed range from 1 to >50, and most data sets incorporate a qualitative description of the grains prior to analysis (e.g., "inclusions," "visible core," or "clear grains"). Recently, BSE images of the grains are typically incorporated as a means to speculate on the textural relationships of the

dated minerals (e.g., Simpson et al. 2000). Some ages have high uncertainties (e.g. 19±72 Ma 17±66 Ma, sample DK2) due to instrumental limitations in measuring small amounts of U. Despite their problematic behavior (Fig. 2), high precision results from Himalayan monazites were primarily responsible for the identification of inheritance (e.g., Copeland et al. 1988) and unsupported daughter products from U disequilibrium (e.g., Schärer 1984, Schärer et al. 1990) and spurred the development and use of other methods to obtain more accurate information from the Himalayas.

Electron microprobe. Numerous studies date monazite using an electron microprobe (e.g., Montel et al. 1996, Bindu et al. 1998, Braun et al. 1998, Cocherie et al. 1998, Finger et al. 1998, Crowley and Ghent 1999, Williams et al. 1999, Martelat et al. 2000, Grew et al. 2002). This *in situ* (= in thin section) methodology allows the preservation of the textural relationships of the grain being dated. Montel et al. (1996) suggest the technique is feasible for >100 Ma monazite, and typical precision is ±30-50 Ma for a total counting time of ~10 min.

Applications of electron-microprobe dating of monazite include exploratory studies as a means (1) to rapidly obtain a large number of ages (Finger and Helmy 1998, Martelat et al. 2000), (2) to identify rocks that experienced a complex geological history, in which several high temperature events are superimposed (Braun et al. 1998, Cocherie et al. 1998, Williams et al. 1999), and/or (3) to obtain age constraints from samples in which textural information is crucial (Finger et al. 1998, Montel et al. 2000).

An example that illustrates the application of electron microprobe dating of monazites is the study of the Beni Bousera granulite. Montel et al. (2000) reported electron-microprobe ages for monazites in metapelites. Monazite grains included in garnet are small (5-20 μm), rare, and difficult to localize in the thin section. Although analytical uncertainties associated with electron microprobe analysis are large, matrix monazites suggest significantly younger ages (Cenozoic) than monazites included in garnet (284±27 Ma). Based on these results, Montel et al. (2000) proposed that monazites entirely included in garnet have the potential to survive granulite facies conditions without being reset.

Ion microprobe. Ion microprobe analysis preserves textural relationships and is thereby ideal for dating monazite grains found in garnet-bearing assemblages (e.g., Harrison et al. 1997a). Using results from the Smith and Giletti (1997) or Cherniak et al. (2002) monazite diffusion studies, a garnet rim P-T data and observations of grain size allow an evaluation of the amount of Pb diffusion possibly experienced by the monazite, thus combining temporal and thermobarometric constraints is a powerful method to obtain the tectonic history. Monazite inclusions in garnet may be further armored against daughter product loss because of the low solubility and permeability of Pb in the host (Montel 1999, Montel et al. 2000).

In situ Th-Pb ion microprobe ages of monazite grains found as inclusions in garnet porphyroblasts and within the deformed rock matrix from samples collected in central Nepal (Catlos et al. 2001), eastern Nepal, and northwest India (Catlos et al. 2002a) indicate the shear zone largely responsible for the creation of the Himalayas was active during the Late Miocene-Pliocene. The age data was combined with P-T estimates from their garnet-bearing assemblages to constrain and develop models for the evolution of the range (e.g., Harrison et al. 1998, Johnson et al. 2001).

Many Himalayan Th-Pb monazite age data are difficult to interpret when results from a single rock are inconsistent with a single population (see also Foster et al. 2000). Monazite growth in metapelites may be due to dissolution of existing detrital grains or allanite breakdown. The dissolution/reprecipitation process is a possible age resetting and

Pb loss mechanism (e.g., Ayers et al. 1999, Townsend et al. 2001) that can be assessed by knowing the textural relationship of the monazite, the distribution of ages within the sample, and the rock's P-T history. Some Himalayan rocks contain evidence of a polyphase history, and dissolution/reprecipitation is speculated to have a strong influence in these samples.

To interpret ion microprobe ages, the P-T history of the rock, textural relationships of the monazite with other phases, uncertainty in the calibration curve, and fraction of Pb* need to be understood. The significance of the age, including those obtained from garnet-hosted and matrix grains, can be judged using models that evaluate potential Pb loss based on temperature, duration conditions, and grain size. Uncertainty in grain size is introduced because the thin section only provides a two-dimensional view of the monazite.

Zhu and O'Nions (1999b) present an example from granulites in Scotland that illustrates the armoring effect of garnet. They report monazite inclusions in garnet that yield U-Pb ages over 1000 Ma older than matrix monazites from the same sample (Zhu and O'Nions 1999b). Catlos (2000) documents an example from the Nepal Himalaya where monazite inclusions in garnet-bearing gneisses yield older ages (late Eocene) than monazites in the matrix (late Oligocene to middle Miocene). Foster et al. (2000) dated matrix monazites (34 to 25 Ma) coexisting with monazite inclusions in garnet (44 to 36 Ma) from a Himalayan metapelite.

The above examples illustrate the importance of textural position for the behavior of the U-Th-Pb system in monazite. Geochronologic studies that employ mineral separation fail to preserve textural relationships between accessory and host phases, and therefore destroy information critical to the interpretation of monazite ages. The common occurrence of monazite as inclusions in garnet provides a unique opportunity to directly date prograde garnet growth. The age patterns revealed between monazites in the matrix of a rock and monazites included in garnet can be used to constrain the timing of garnet growth. If monazite inclusions show an age progression from core to rim of their garnet host, monazite likely grew synchronously with garnet.

U-TH-PB DATING OF APATITE

Apatite has been dated by U-Pb ion microprobe (Sano et al. 1999a,b; Sano and Terada 1999), isotope dilution techniques (e.g., Romer 1996, Corfu and Stone 1998, Chamberlain and Bowring 2000), and laser ablation-inductively coupled plasma-mass spectrometry (Willigers et al. 2002). Low U content (~<50 ppm, see Fig. 11) and high Pb° (e.g., Corfu and Stone 1998) hinders apatite U-Pb dating. Pb° issues are addressed in isotope dilution studies by using the isotopic composition of coexisting feldspar as an approximation for the initial Pb in the apatite grain (Corfu and Stone 1998, Chamberlain and Bowring 2000, Corfu and Easton 2000). Corfu and Stone (1998) suggest that there is "no insurance" that Pb in related minerals is the same as that incorporated into the apatite, but Chamberlain and Bowring (2000) advocate the method as a "good approximation…in many geologic settings". Although Corfu and Easton (2000) report 15-19% precision for U-Pb ages of Precambrian(?) apatites, Chamberlain and Bowring (2000) obtained precisions for apatite U-Pb ages varying from ±1.2% to ±0.3% for Proterozoic or Archean grains. Mougeot et al. (1997) reports a precise age of French Massif Velay anatectic dome apatite grains dated using isotope dilution of 289±5 Ma, and suggest the age times the end of the thermal event. Rakovan et al. (1997) were able to date a bulk reference apatite (American Museum of Natural History #69739) as well as its crystal faces using Sm/Nd isotope dilution techniques, and outline a methodology that could be potentially applicable to U-Th-Pb dating.

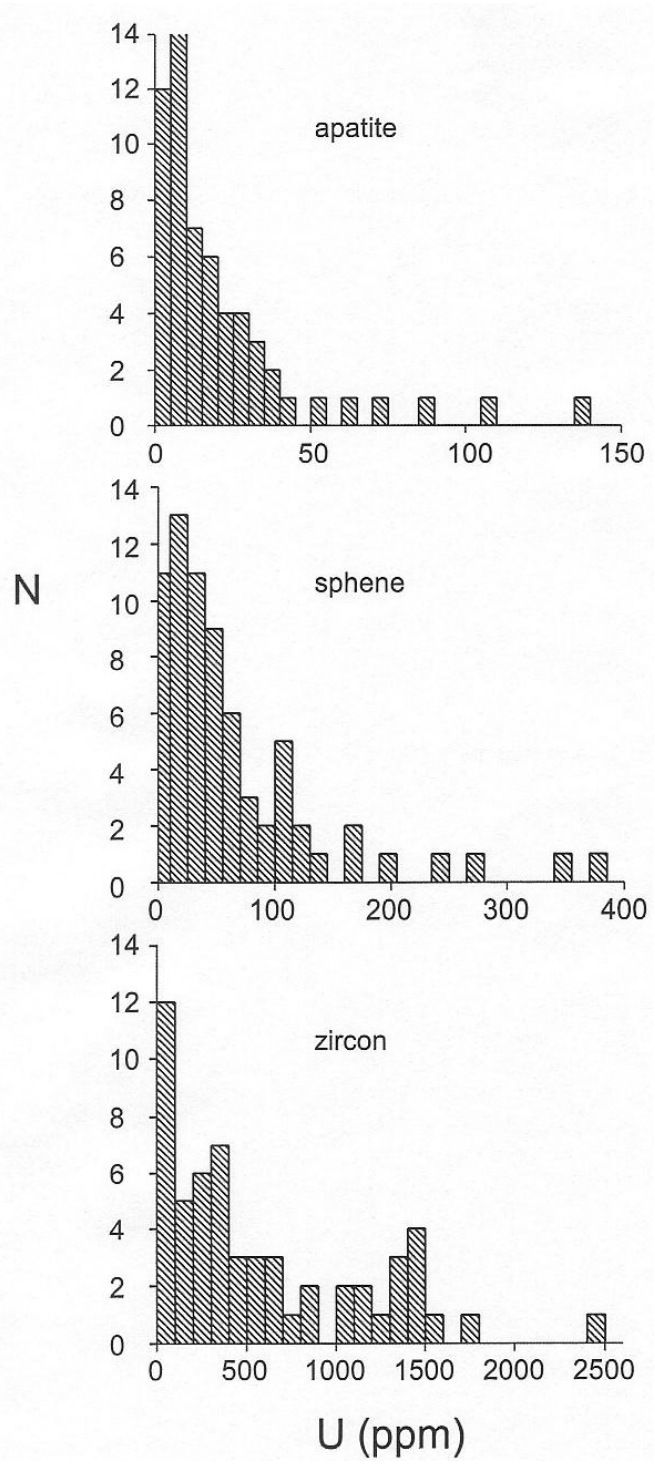

Figure 11. U concentrations (ppm) of apatite, sphene, and zircon from Romer (1996), Corfu and Stone (1998), Chamberlain and Bowring (2000), and Corfu and Easton (2000).

Sano et al. (1999a) report 3-5% precisions for apatite ages obtained using an ion microprobe. Sano and Terada (1999) used the method to date a fossil shark tooth and obtained a ^{238}U-^{206}Pb isochron age of 266±18 Ma, consistent with the highly imprecise ^{235}U-^{207}Pb age of 453±170 Ma and Th-Pb age of 235±310 Ma. Sano et al. (1999b) used the ion microprobe to date zircon and apatite grains from the Acasta Gneiss, Canada. The apatite ages are ~3 Ga younger than the zircon crystallization ages or correspond closely to the lower concordia intercept defined by some zircon analyses, suggesting that apatite records a later thermal event.

Willigers et al. (2002) report apatite and monazite ages from Paleoproterozoic metamorphic rocks from West Greenland obtained using laser-ablation inductively-coupled plasma mass spectrometry. Their ages were identical to those determined by isotope dilution, but also measured more Pb* the solution-based isotope dilution. Willigers et al. (2002) suggest *in situ* analysis eliminates the need for mineral separation, thus limiting the potential of Pb° contamination during separation, chemical digestion and/or analysis.

U-TH-PB DATING OF XENOTIME

Xenotime is commonly dated using isotope dilution methods (e.g., Schärer et al. 1990, Hawkins and Bowring 1997, 1999; Graessner et al. 2000), and, more recently, by ion microprobe techniques (Kamber et al. 1998, McNaughton et al. 1999, Petersson et al. 2001) and electron microprobe methods (Suzuki and Adachi 1991, Griffen et al. 2000, Asami et al. 2002, Grew et al. 2002). To aid in age interpretation, monazite is commonly analysed from the same rock or locality. Gehrels and Smith (1991) obtained a

concordant age of 51±2 Ma for isotope dilution analyses of monazite and xenotime fractions collected from a Southern Arizona leucogranite, suggesting that these minerals record temporally similar closure temperature or crystallization events. Table 4 lists xenotime and monazite ages obtained by several workers. Himalayan monazites and xenotimes often yield different ages (Hodges et al. 1992, Simpson et al. 2000, Viskupic and Hodges 2001), probably because these grains were collected from lithologies that experienced complicated metamorphic histories (e.g., Le Fort 1996), thus recording multiple magmatic or metamorphic events, inheritance or Pb loss. Kamber et al. (1998) report older ages of xenotime inclusions in cordierite (2612±8 Ma) compared to those in the matrix (2551±5 Ma), and suggest that matrix grains were exposed to subsequent Pb loss via diffusion. Preservation of textural relationships of dated grains is key for deciphering the significance of the xenotime age.

Table 4. Summary of U-Pb analytical data from monazite and xenotime.[a]

Locality	*Xenotime age (Ma)*	*Monazite age (Ma)*
	$^{207}Pb/^{208}Pb$ (±2σ)	$^{207}Pb/^{208}Pb$ (±2σ)
	Hawkins & Bowring (1997)	
Grand Canyon	1676 (1)	1673 (1)
Grand Canyon	1681 (1)	1678 (2)
	Kamber et al. (1998)	
Limpopo	2612 (8)	2600 (7)
	Hawkins & Bowring (1999)	
Grand Canyon	1698 (1)	1698 (1)
	$^{207}Pb/^{235}U$ (±2σ)	$^{207}Pb/^{235}U$ (±2σ)
	Schärer et al. (1990)	
Ailao Shan	23.1 (0.3)	22.7 (0.3)
	Hodges et al. (1992)	
□33 Himalaya	21.1 (0.1)	21[b]
	Schärer et al. (1994)	
Diangcan Sahn	22.4 (0.1)	24.2 (0.2)
Jianchuan	23.0 (0.2)	22.7 (0.3)
	Hodges et al. (1996)	
Himalaya	23.4 (0.1)	35.6 (0.1)
	Schärer et al. (1996)	
Isorno-Orselina	24.7 (0.3)	26.5 (0.6)
	Simpson et al. (2000)	
21.0 (0.4)	44.2 (0.5)	
Himalaya[c]	21.0 (0.4)	20.3 (0.5)
	Viskupic & Hodges (2001)	
Himalaya	99.8 (0.4)	42.5 (0.5)
Himalaya[c]	22.3 (0.6)	24.1 (0.1)
	$^{206}Pb/^{238}U$ (±2σ)	$^{206}Pb/^{238}U$ (±2σ)
	Eliasson & Schoberg (1991)	
Bohus Granite	919 (10)	922 (10)

a. All analyses were obtained using isotope dilution methods, except Kamber et al. (1998) who analyzed the minerals using an ion microprobe.

b. Analyses by Copeland et al. (1988).

c. Average ages of only the Miocene grains.

SUMMARY

The widespread occurrence in crustal rocks of the accessory phosphate minerals apatite, monazite, and xenotime, their tendency to concentrate U and Th and exclude Pb, their generally high degree of retentivity of daughter Pb, and their resilience to radiation damage, make them excellent candidates as geochronometers. Furthermore, the restricted range of monazite stability provides a uniquely capable thermochronometer for understanding dynamic crustal processes. The various methodologies used to obtain U-Th-Pb ages each have certain attractions and limitations. Isotope dilution potentially provides high precision but with an accompanying loss of textural information. The electron microprobe is widely available and has high spatial resolution, but has poor precision and requires assumptions that cannot be rigorously tested without isotopic data. The ion microprobe has both high spatial resolution and *in situ* analysis capability but is restricted to a minimum inter-element precision of ~1%. Laser ablation inductively coupled plasma mass spectrometry promises high spatial resolution with precision potentially comparable to conventional isotope dilution studies. Depending on the application, the preferred approach is one that combines the best balance between spatial resolution, textural and sample preservation, precision, and accuracy.

REFERENCES

Ahrens LH (1955) The convergent lead ages of the oldest monazites and uraninites (Rhodesia, Manitoba, Madagascar, and Transvaal). Geochim Cosmochim Acta 7:294-300

Aldrich LT, Tilton GR, Davis GL, Nicolaysen LO, Patterson CC (1955) Comparison of U-Pb and Pb-Pb and Rb-Sr ages of Precambrian minerals. *In* Symposium on Precambrian Correlation and Dating. Vol. 7. Derry DR (ed) Canadian Geol Assoc, p 7-13

Aldrich LT, Davis GL, Tilton GR, Wetherill GW (1956) Radioactive ages of minerals from the Brown Derby Mine and the Quartz Creek Granite near Gunnison, Colorado. J Geophys Res 61:215-232

Ancey M, Bastenaire F, Tixier R (1978) Application des méthodes statistiques en microanalyse. *In* Microanalyse, microscopie electronique à balayage. Maurice F, Meny L, Tixier R (eds) Les Editions du Physicien Orsay, France, p 323-347

Asami M, Suzuki K, Grew ES (2002) Chemical Th-U-total Pb dating by electron microprobe analysis of monazite, xenotime, and zircon from the Archean Napier Complex, East Antarctica: Evidence for ultra-high-temperature metamorphism at 2400 Ma. Precambrian Res 114:249-275

Ayers JC, Miller C, Gorisch B, Milleman J (1999) Textural development of monazite during high-grade metamorphism: Hydrothermal growth kinetics, with implications for U, Th-Pb geochronology. Am Mineral 84:1766-1780

Bea F, Montero P (1999) Behavior of accessory phases and redistribution of Zr, REE, Y, Th, and U during metamorphism and partial melting of metapelites in the lower crust: An example from the Kinzigite Formation of Ivrea-Verbano, NW Italy. Geochim Cosmochim Acta 63:1133-1153

Bindu RS, Yoshida M, Santosh M (1998) Electron microprobe dating of monazite from the Chittikara Granulite, South India: Evidence for polymetamorphic events. J Geosci 41:77-83

Bingen B, Van Bremen O (1998) U-Pb monazite ages in amphibolite- to granulite-facies orthogneiss reflect hydrous mineral breakdown reactions: Sveconorwegian Province of SW Norway. Contrib Mineral Petrol 132:336-353

Black LP, Fitzgerald JD, Harley SL (1984) Pb isotopic composition, colour, and microstructure of monazites from a polymetamorphic rock in Antarctica. Contrib Mineral Petrol 85:141-148

Braun I, Montel J-M, Nicollet C (1998) Electron microprobe dating of monazites from high-grade gneisses and pegmatites of the Kerala Khondalite Belt, southern India. Chem Geol 146:65-85

Bruhn F, Moller A, Sie SH, Hensen BJ (1999) U-Th-Pb chemical dating of monazites using the proton microprobe. Nucl Instr Meth Phys Res B 158:616-620

Burger AJ, Nicolaysen LO, Ahrens LH (1967) Controlled leaching of monazites. J Geophys Res 72: 3585-3594

Burt DM (1989) Compositional and phase relations among rare earth element minerals. Rev Mineral 21:259-307

Carslaw HS, Jaeger JC (1959) Conduction of Heat in Solids, 2nd edn. Clarendon, Oxford, UK

Catlos EJ (2000) Thermobarometric and geochronologic constraints on the evolution of the Main Central Thrust, Himalayan orogen. PhD dissertation, University of California, Los Angeles, California

Catlos EJ, Gilley LD, Harrison TM (in press, 2002b) Interpretation of monazite ages obtained via *in situ* analysis. Chem Geol

Catlos EJ, Harrison TM, Kohn, MJ, Grove M, Ryerson FJ, Manning CE, Upreti BN (2001) Geochronologic and thermobarometric constraints on the evolution of the Main Central Thrust, central Nepal Himalaya. J Geophys Res 106:16177-16204

Catlos EJ, Harrison TM, Manning CE, Grove M, Rai SM, Hubbard MS, Upreti BN (2002a) Records of the evolution of the Himalayan orogen from in situ Th-Pb ion microprobe dating of monazite: Eastern Nepal and Garhwal. J Asian Earth Sci 20:459-479

Chamberlain KR, Bowring SA (2000) Apatite-feldspar U-Pb thermochronometer: A reliable, mid-range (~450°C), diffusion-controlled system. Chem Geol 172:173-200

Cheburkin AK, Frei R, Shotyk W (1997) An energy-dispersive miniprobe multielement analyzer (EMMA) for direct analysis of trace elements and chemical age dating of single mineral grains. Chem Geol 135:75-87

Cherniak DJ, Lanford WA, Ryerson FJ (1991) Pb diffusion in apatite and zircon using ion implantation and Rutherford backscattering techniques. Geochim Cosmochim Acta 55:1663-1673

Cherniak DJ, Watson EB, Grove M, Harrison TM (2002) Pb diffusion in monazite (manuscript)

Cherniak DJ, Watson EB, Harrison TM, Grove M (2000) Pb diffusion in monazite: A progress report on a combined RBS/SIMS study. EOS Trans, Am Geophys Union 81:S25

Cocherie A, Albarède F (2001) An improved U-Th-Pb age calculation for electron microprobe dating of monazite. Geochim Cosmochim Acta 65:4509-4522

Cocherie A, Legendre O, Peucat JJ, Kouamelan AN (1998) Geochronology of polygenetic monazites constrained by in situ electron microprobe Th-U-total lead determination: Implications for lead behaviour in monazite. Geochim Cosmochim Acta 62:2475-2497

Coleman ME (1998) U-Pb constraints on Oligocene-Miocene deformation and anatexis within the central Himalaya, Marsyandi Valley, Nepal. Am J Sci 298:553-571

Compston W, Williams IS, Meyer C (1984) U-Pb geochronology of zircons from Lunar Breccia 73217 using a sensitive, high mass resolution ion microprobe: Proceedings of the 14th Lunar and Planetary Science Conference, Part 2. J Geophys Res 89:8525-8534

Copeland P, Parrish RR, Harrison TM (1988) Identification of inherited radiogenic Pb in monazite and its implications for U-Pb systematics. Nature 333:760-763

Corfu F, Easton RM (2000) U-Pb evidence for polymetamorphic history of Huronian rocks within the Grenville front tectonic zone east of Sudbury, Ontario, Canada. Chem Geol 172:149-171

Corfu F, Stone D (1998) The significance of titanite and apatite U-Pb ages: Constraints for the post-magmatic thermal-hydrothermal evolution of a batholitic complex, Berens River area, northwestern Superior Province, Canada. Geochim Cosmochim Acta 62:2979-2995

Crank J (1975) The Mathematics of Diffusion. Oxford University Press, New York

Crowley JL, Ghent ED (1999) An electron microprobe study of the U-Th-Pb systematics of metamorphosed monazite: The role of Pb diffusion versus overgrowth and recrystallization. Chem Geol 157:285-302

Dahl PS (1997) A crystal-chemical basis for Pb retention and fission-track annealing systematics in U-bearing minerals, with implications for geochronology. Earth Planet Sci Lett 150:277-290

Davis DW, Krogh TE (2000). Preferential dissolution of ^{234}U and radiogenic Pb from a-recoil damages lattice sites in zircon: Implications for thermal histories and Pb-isotopic fractionation in the near-surface environment. Chem Geol 172:41-58

Deer WA, Howie RA, Zussman J (1992) An Introduction to the Rock-Forming Minerals, 2nd edn. Longman Scientific and Technical Press, Essex, UK

Deniel C, Vidal P, Fernandez A, Le Fort P, Peucat JJ (1987) Isotopic study of the Manaslu granite (Himalaya, Nepal): Inferences on the age and source of the Himalayan leucogranites. Contrib Mineral Petrol 96:78-92

DeWolf CP, Belshaw N, O'Nions RK (1993) A metamorphic history from micron-scale $^{207}Pb/^{206}Pb$ chronometry of Archaean monazite. Earth Planet Sci Lett 120:207-220

Dodson MH (1973) Closure temperature in cooling geochronological and petrological systems. Contrib Mineral Petrol 40:259-274

Edwards MA, Harrison TM (1997) When did the roof collapse? Late Miocene north-south extension in the High Himalaya revealed by Th-Pb monazite dating of the Khula Kangri granite. Geology 25:543-546

Eliasson T, Schoberg H (1991) U-Pb dating of the post-kinematic Sveconorwegian (Grenvillian) Bohus Granite, SW Sweden: Evidence for restitic zircon. Precambrian Res 51:337-350

Engi M, Scherrer NC, Burri T (2001) Metamorphic evolution of pelitic rocks of the Monte Rosa nappe: Constraints from petrology and single grain monazite age data. Schweiz mineral petrogr Mitt 81: 305-328

England GL, Rasmussen B, McNaughton NJ, Fletcher IR, Groves DI, Krapez B (2001) SHRIMP U-Pb ages of diagenetic and hydrothermal xenotime from the Archaean Witwatersrand Supergroup of South Africa. Terra Nova 13:360-367

Ewing RC (1994) The metamict state: 1993 the centennial. Nucl Inst Meth Phys Res B 91:22-29

Faure G (1986) Principles of Isotope Geology, 2nd ed. John Wiley and Sons, New York

Fenner CN (1928) The analytical determination of uranium, thorium, and lead as a basis for age-calculations. Am J Sci 26:369-381

Fenner CN (1932) Radioactive minerals from Divino de Uba, Brazil. Am J Sci 23:382-391

Ferry JM (2000) Patterns of mineral occurrence in metamorphic rocks. Am Mineral 85:1573-1588

Fick A (1855) Ueber diffusion. Ann Phys Chem 94:59-86

Finger F, Broska I, Roberts, MP, Schermaier A (1998) Replacement of primary monazite by apatite-allanite-epidote coronas in an amphibolite facies granite gneiss from the eastern Alps. Am Mineral 83:248-258

Finger F, Helmy HM (1998) Composition and total-Pb model ages of monazite from high-grade paragneisses in the Abu Swayel area, southern Eastern Desert, Egypt. Mineral Petrol 62:269-289

Förster HJ (1998a) The chemical composition of REE-Y-Th-U-rich accessory minerals in peraluminous granites of the Erzgebirge-Fichtelgebirge region, Germany, Part I: The monazite-(Ce)-brabantite solid solution series. Am Mineral 83:259–272

Förster HJ (1998b) The chemical composition of REE-Y-Th-U-rich accessory minerals in peraluminous granites of the Erzgebirge-Fichtelgebirge region, Germany. Part II: Xenotime. Am Mineral 83:1302–1315

Foster G, Kinny P, Vance D, Prince C, Harris N (2000) The significance of monazite U-Th-Pb age data in metamorphic assemblages: A combined study of monazite and garnet chronometry. Earth Planet Sci Lett 181:327-340

Gehrels GE, Smith CH (1991) U-Pb geochronological constraints on the age of thrusting, crustal extension, and peraluminous plutonism in the Little Rincon Mountains, southern Arizona. Geology 19:238-241

Geisler T, Schleicher H (2000) Improved U–Th–total-Pb dating of zircons by electron microprobe using a simple new background modeling procedure and Ca as a chemical criterion of fluid-induced U–Th–Pb discordance in zircon. Chem Geol 163:269-285

Gilley LD (2001) Timing of left-lateral shearing and prograde metamorphism along the Red River Shear Zone, China and Vietnam. PhD Dissertation, University of California, Los Angeles, California

Gilley LD, Harrison TM, Leloup PH, Ryerson FJ, Lovera OM, Wang J-JH (submitted, 2002) Direct dating of left-lateral deformation along the Red River shear zone, China and Vietnam. J Geophys Res

Gleadow AJW, Duddy IR, Lovering JF (1983) Fission track analysis: A new tool for the evaluation of thermal histories and hydrocarbon potential. Aust Petrol Explor Assoc J 23:93-102

Gottfried D, Jaffe HW, Senftle FE (1959) Evaluation of the lead-alpha (Larsen) method for determining ages of igneous rocks. Geol Surv Bull B 1097-A:1-63

Graessner T, Schenk V, Brocker M, Mezger K (2000) Geochronological constraints on the timing of granitoid magmatism, metamorphism, and post-metamorphic cooling in the Hercynian crustal cross-section of Calabria. J Metamorph Geol 18:409-421

Grew ES, Kazuhiro S, Masao A (2002) CHIME ages of xenotime, monazite, and zircon from beryllium pegmatites in the Napier Complex, Khmara Bay, Enderby Land, East Antarctica. Polar Geosci 14: 99-118

Griffen BJ, Forbes D, McNaughton NJ (2000) Evaluation of dating of diagenetic xenotime by electron microprobe. Microsc Microanal 6 Suppl 2:408-409

Grove M, Harrison TM (1999) Monazite Th-Pb age depth profiling. Geology 27:487–490

Harrison TM, Grove M, Lovera OM (1997b) New insights into the origin of two contrasting Himalayan granite belts. Geology 25:899-902

Harrison TM, Grove M, Lovera OM, Catlos EJ (1998) A model for the origin on Himalayan anatexis and inverted metamorphism. J Geophys Res 103:27017-27032

Harrison TM, Grove M, Lovera OM, Catlos EJ, D'Andrea J (1999b) The origin of Himalayan anatexis and inverted metamorphism: Models and constraints. J Asian Earth Sci 17:755-772

Harrison TM, Grove M, McKeegan KD, Coath CD, Lovera OM, Le Fort P (1999a) Origin and emplacement of the Manaslu intrusive complex, Central Himalaya. J Petrol 40:3-19

Harrison TM, McKeegan KD, Le Fort P (1995) Detection of inherited monazite in the Manaslu leucogranite by $^{208}Pb/^{232}Th$ ion microprobe dating: Crystallization age and tectonic implications. Earth Planet Sci Lett 133:271-282

Harrison TM, Ryerson FJ, Le Fort P, Yin A, Lovera OM, Catlos EJ (1997a) A Late Miocene-Pliocene origin for central Himalayan inverted metamorphism. Earth Planet Sci Lett 146:E1-E8

Harrison TM, Watson EB (1984) The behavior of apatite during crustal anatexis: Equilibrium and kinetic considerations. Geochim Cosmochim Acta 48:1467-1477

Hawkings DP, Bowring SA (1997) U-Pb systematics of monazite and xenotime: Case studies from the Paleoproterozoic of the Grand Canyon, Arizona. Contrib Mineral Petrol 127:87-103
Hawkings DP, Bowring SA (1999) U-Pb monazite, xenotime, and titanite geochronological constraints on the prograde to post-peak metamorphic thermal history of Paleoproterozoic migmatites from the Grand Canyon, Arizona. Contrib Mineral Petrol 134:150-169
Hodges KV, Parrish RR, Housh TB, Lux DR, Burchfiel BC, Royden LH, Chen Z (1992) Simultaneous Miocene extension and shortening in the Himalayan orogen. Science 258:1466-1470
Hodges KV, Parrish RR, Searle MP (1996) Tectonic evolution of the central Annapurna Range, Nepalese Himalayas. Tectonics 15:1264-1291
Holmes A (1911) The association of lead with uranium in rock-minerals and its application to the measurement of geological time. Proc Roy Soc London A 85:248-256
Holmes A (1954) The oldest dated minerals of the Rhodesian Shield. Nature 173:612
Holmes A (1955) Dating the Precambrian of peninsular India and Ceylon. Proc Geol Soc Canada 7:81-106
Holmes A, Cahen L (1955) African geochronology. Col Geol Min Res 5:3-38
Holmes A, Smales AA, Leland WT, Nier AO (1949) The age of uraninite and monazite from the post-Delhi pegmatites of Rajputana. Geol Mag 86:288-302
Iskanderova AD, Legiyerskiy Y (1966) Use of apatite for determination of the absolute age of geological formations by the lead-isotope method. Akad Nauk SSSR Kom Opred Absol Vozrasta Geol Form Tr 13:444-448
Johnson MRW, Oliver GJH, Parrish RR, Johnson SP (2001) Synthrusting metamorphism, cooling, and erosion of the Himalayan Kathmandu complex, Nepal. Tectonics 20:394-415
Kamber BS, Frei R, Gibb AJ (1998) Pitfalls and new approaches in granulite chronometry: An example from Limpopo Belt, Zimbabwe. Precambrian Res 91:269-285
Karioris FG, Gowda K, Cartz L (1981) Heavy ion bombardment on monoclinic $ThSiO_4$, ThO_2, and monazite. Radiat Eff Lett 58:1-3
Kingsbury JA, Miller CF, Wooden JL Harrison TM (1993) Monazite paragenesis and U-Pb systematics in rocks of the eastern Mojave Desert, California, USA: Implications for thermochronometry. Chem Geol 110:147-167
Kohn MJ, Catlos EJ, Ryerson FJ, Harrison TM (2001) P-T-t path discontinuity in the MCT Zone, Central Nepal. Geology 29:571-574
Köppel V, Grünenfelder M (1975) Concordant U-Pb ages of monazite and xenotime from the central Alps and the timing of the high temperature Alpine metamorphism, a preliminary report. Schweiz mineral petrogr Mitt 55:129-132
Köppel V, Gunthert A, Grünenfelder M (1980) Patterns of U-Pb zircon and monazite ages in polymetamorphic units of the Swiss Central Alps. Schweiz mineral petrogr Mitt 61:97-119
Kosler J, Tubrett MN, Sylvester PJ (2001) Application of laser ablation ICP-MS to U-Th-Pb dating of monazite. Geostand Newslett 25:375-386
Krogstad EJ, Walker RJ (1994) High closure temperatures of the U-Pb system in large apatites from the Tin Mountain pegmatite, Black Hills, South Dakota, USA. Geochim Cosmochim Acta 58:3845-3853
Larsen ES, Keevil NB, Harrison HC (1949) Preliminary report on determining the age of rocks by the lead-uranium ration of zircon, apatite, and sphene from the rocks using alpha counting and spectrographic methods. *In* Report of the Committee on Measurement of Geologic Time. National Research Council, Div Geol Geogr Ann Rep E, 1947-1948. Marble JP (ed) American Geological Institute, p 27-28
Le Fort P (1996) Evolution of the Himalaya. *In* The Tectonic Evolution of Asia. Yin A, Harrison TM (eds) Cambridge University Press, New York, p 95-109
Lyakhovich VV (1961) Accessory minerals and the absolute age of igneous rocks. Trudy Inst Mineral Geokhim Krisallokhim Redkikh Elementov 7:212-225
Machado N, Gauthier G (1996) Determination of $^{207}Pb/^{206}Pb$ ages on zircon and monazite by laser-ablation ICPMS and application to a study of sedimentary provenance and metamorphism in southeastern Brazil. Geochim Cosmochim Acta 60:5063-5073
Marble JP (1935) Possible age of monazite from Mars Hill, North Carolina. Am Mineral 21:724-732
Martelat J-E, Lardeaux J-M, Nicollet C, Rakotondrazafy R (2000) Strain pattern and late Precambrian deformation history in southern Madagascar. Precambrian Res 102:1-20
Mattinson JM (1994) A study of complex discordance in zircons using step-wise dissolution techniques. Contrib Mineral Petrol 116:117-129
McNaughton NJ, Rasmussen B, Fletcher IR (1999) SHRIMP uranium-lead dating of diagenetic xenotime in siliclastic sedimentary rocks. Science 285:78-80
Meldrum A, Boatner LA, Ewing RC (1997b) Displacive radiation effects in the monazite- and zircon-structure orthophosphates. Phys Rev B 56:13805-13814
Meldrum A, Boatner LA, Ewing RC (1997c) Electron-irradiation-induced nucleation and growth in amorphous $LaPO_4$, $ScPO_4$, and zircon. J Mater Sci 12:1816-1827

Meldrum A, Boatner LA, Wang LM, Ewing RC (1997a) Ion-beam-induced amorphisation of $LaPO_4$ and $ScPO_4$. Nucl Instr Meth B 127/128:160-165

Meldrum A, Boatner LA, Weber WJ, Ewing RC (1998) Radiation damage in zircon and monazite. Geochim Cosmochim Acta 62:2509-2520

Meldrum A, Wang LM, Ewing RC (1996) Ion beam induced amorphization of monazite. Nucl Instr Meth Phys Res B 116:220-224

Michot J, Deutsch S (1970) U-Pb zircon ages and polycylism of the Gneiss de Brest and the adjacent formations (Brittany). Eclog Geol Helv 63:215-227

Montel J-M (1993) A model for monazite/melt equilibrium and application to the generation of granitic magmas. Chem Geol 110:127-146

Montel J-M (1999) Some good reasons for monazite to be concordant. J Conf Abstr EUG 10 4:800

Montel JM, Devidal JL, Avignant, DC (2002, in press) X-ray diffraction study of brabantite-monazite solid solution. Chem Geol

Montel J-M, Foret S, Veschambrem M, Nicollet C, Provost A (1996) Electron microprobe dating of monazite. Chem Geol 131:37-53

Montel J-M, Kornprobst J, Vielzeuf D (2000). Preservation of old U-Th-Pb ages in shielded monazite: Example from Beni Bousera Hercynian kinzigites (Morocco). J Metamorph Geol 18:335-342

Montel J-M, Veschambrem M, Nicollet C (1994) Datation de la monazite à la microsonde électronique. C R Acad Sci Paris 318:1489

Mougeot R, Respaut JP, Ledru P, Marignac C (1997) U-Pb geochronology on accessory minerals of the Velay anatectic Dome (French Massif Central). Eur J Mineral 9:141-156

Nazarchuk JH (1993) Structure and geochronology of the Greater Himalaya, Kali Gandaki region, west-central Nepal. Masters Thesis, Carleton University, Ottawa, Ontario

Ni Y, Hughes JM, Mariano A (1995) Crystal chemistry of the monazite and xenotime structures. Am Mineral 80:21-26

Nier AO (1939) The isotopic constitution of radiogenic lead and the measurement of geologic time, II. Phys Rev 55:153-163

Nier AO, Thompson RW, Murphy BF (1941) The isotopic composition of lead and the measurement of geologic time, III. Phys Rev 60:789-793

Olsen SN, Livi K (1998) Dating of monazite from migmatites in the Aar Massif, Swiss Alps, by electron microprobe analyses. Abstr Geol Soc Am 30:231

Ouchani S, Dran JC, Chaumont J (1997) Evidence of ionization annealing upon helium-irradiation of pre-damaged fluorapatite. Nucl Instr Meth Phys Res B 132:447-451

Overstreet WC (1967) The geologic occurrence of monazite. U S Geol Surv Prof Pap 530:1-327

Paquette JL, Montel J-M, Chopin C (1999) U-Th-Pb dating of the Brossasco ultrahigh-pressure metagranite, Dora-Maira massif, western Alps. Eur J Mineral 11:69-77

Parrish RR (1990) U-Pb dating of monazite and its application to geological problems. Can J Earth Sci 27:1431-1450

Parrish RR, Armstrong RL (1987) The ca. 162 Ma Galena Bay Stock and its relationship to the Columbia River fault zone, southeast British Columbia. Radiogenic age and isotopic studies, Geol Surv Canada Rep 1 87-2:25-32

Parrish RR, Hodges KV (1996) Isotopic constraints on the age and provenance of the Lesser and Greater Himalaya sequences, Nepalese Himalaya. Geol Soc Am Bull 108:904-911

Pêcher A, Le Fort P (1986) The metamorphism in central Himalaya, its relations with the thrust tectonic. *In* Évolution des domains orogéniques d'Asie méridionale (de la Turquie à l'Indoneasie) Le Fort P, Colchen M, Montenat C (eds) Science de la Terre 47, p 285-309

Parrish RR, Tirrul R (1989) U-Pb age of the Baltoro granite, northwest Himalaya, and implications for monazite U-Pb systematics. Geology 17:1076-1079

Peiffert C, Cuney M (1999) hydrothermal synthesis of the complete solid solution between monazite ($LaPO_4$) and huttonite ($ThSiO_4$) at 780°C and 200 MPa. J Conf Abstr EUG 10 4:522

Petersson J, Whitehouse MJ, Eliasson T (2001) Ion microprobe U-Pb dating of hydrothermal xenotime from an episyenite: Evidence for rift-related reactivation. Chem Geol 175:703-712

Podor R, Cuney M (1997) Experimental study of Th-bearing $LaPO_4$ (780°C, 200 MPa): Implication for monazite and actinide orthophosphate stability. Am Mineral 82:765-771

Podor R, Cuney M, Nguyen TC (1995) Experimental study of the solid solution between monazite-(La) and $Ca_{0.5}U_{0.5}PO_4$ at 780°C and 200 MPa. Am Mineral 80:1261-1268

Poitrasson F, Chenery S, Bland DJ (1996) Contrasted monazite hydrothermal alteration mechanisms and their geochemical implications. Earth Planet Sci Lett 145:79-96

Poitrasson F, Chenery S, Shepherd T (2000) Electron microprobe and LA-ICP-MS study of monazite hydrothermal alteration: Implications for U-Th-Pb geochronology and nuclear ceramics. Geochim Cosmochim Acta 64:3283-3297

Pyle J, Spear FS (1999) Yttrium zoning in garnet: Coupling of major and accessory phases during metamorphic reactions. Geol Mater Res 1:1-49

Quarton M, Zouiri M, Freundlich W (1994) Cristallochimie des orthophosphates doubles de thorium et de plomb. C R Acad Sci Paris 229:785-788

Rakovan J, McDaniel DK, Reeder R (1997) Use of surface-controlled REE sectoral zoning in apatite from Llallagua, Bolivia, to determine a single-crystal Sm-Nd age. Earth Planet Sci Lett 146:329-336

Rapp RP, Watson EB (1986) Monazite solubility and dissolution kinetics: Implications for the thorium and light rare-earth chemistry of felsic magmas. Contrib Mineral Petrol 94:304-316

Rasmussen B, Fletcher IR, McNaughton NJ (2001) Dating low-grade metamorphic events by SHRIMP U-Pb analysis of monazite in shales. Geology 29:963–966

Rhede D, Wendt I, Forster H-J (1996) A three-dimensional method for calculating independent chemical U/Pb- and Th/Pb-ages of accessory minerals. Chem Geol 130:247-253

Robinson A, Yin A, Manning CE, Harrison TM, Hei W, Xiong MY, Feng, WX (2001) Geochronologic, thermochronologic, and thermobarometric constraints on the tectonic evolution of the northeastern Pamir. EOS Trans, Am Geophys Union 82:T11E-0888

Romer RL (1996) U-Pb systematics of stilbite-bearing low-temperature mineral assemblages from the Malmberget iron ore, northern Sweden. Geochim Cosmochim Acta 60:1951-1961

Ryerson FJ (1987) Diffusion Measurements: Experimental Methods. *In* Methods of Experimental Geophysics. Vol. 24. Sammis CG, Henyey T (eds) Academic Press, New York, p 89-129

Sano Y, Oyama T, Terada K, Hidaka H (1999a) Ion microprobe dating of apatite. Chem Geol 153:249-258

Sano Y, Terada K (1999) Direct ion microprobe U-Pb dating of fossil tooth of a Permian shark. Earth Planet Sci Lett 174:75-80

Sano Y, Terada K, Hidaka H, Yokoyama K, Nutman AP (1999b) Palaeoproterozoic thermal events recorded in the ~4.0-Ga Acasta gneiss, Canada: Evidence from SHRIMP U-Pb dating of apatite and zircon. Geochim Cosmochim Acta 63:899-905

Schärer U (1984) The effect of initial ^{230}Th disequilibrium on young U-Pb ages: The Makalu case, Himalaya. Earth Planet Sci Lett 67:191-204

Schärer U, Cosca M, Steck A, Hunziker J (1996) Termination of major ductile strike-slip shear and differential cooling along the Insubric line (central Alps): U-Pb, Rb-Sr, and ^{40}Ar/^{39}Ar ages of cross-cutting pegmatites. Earth Planet Sci Lett 142:331-351

Schärer U, Tapponier P, Lacassin R, Leloup PH, Dalai Z, Shaocheng J (1990) Intraplate tectonics in Asia: A precise age for large-scale Miocene movement along the Ailao Shan-Red River shear zone, China. Earth Planet Sci Lett 97:65-77

Schärer U, Xu RH, Allegre CJ (1986) U-(Th)-Pb systematics and ages of Himalayan leucogranites, South Tibet. Earth Planet Sci Lett 77:35-48

Schärer U, Zhang LS, Tapponier P (1994) Duration of strike-slip movements in large shear zones: The Red River belt, China. Earth Planet Sci Lett 126:379-397

Scherrer NC, Engi M, Gnos E, Jakob V, Liechti A (2000) Monazite analysis: From sample preparation to microprobe age dating and REE quantification. Schweiz mineral petrogr Mitt 80:93-105

Searle MP, Parrish RR, Hodges KV, Hurford A, Ayers MW, Whitehouse MJ (1997) Shisha Pangma leucogranite, South Tibetan Himalaya: Field relations, geochemistry, age, origin, and emplacement. J Geol 105:295-317

Seydoux-Guillaume AM, Wirth R, Nasdala L, Gottschalk M, Montel J-M, Heinrich W (2002) An XRD, TEM and Raman study of experimentally annealed natural monazite. Phys Chem Min 29:240-253

Shestakov GI (1969) On diffusional loss of lead from a radioactive mineral. Trans Geok 9:1103-1111

Simpson RL, Parrish RR, Searle MP, Waters DJ (2000) Two episodes of monazite crystallization during metamorphism and crustal melting in the Everest region of the Nepalese Himalaya. Geology 28: 403-406

Sivaramakrishnan V, Venkatasubramaniam VS (1959) Ages of some detrital monazites by the lead-alpha method of geochronology. Proc Nat Inst Sci India A Phys Sci 25:278-280

Smith HA, Barreiro B (1990) Monazite U-Pb dating of staurolite grade metamorphism in pelitic schists. Contrib Mineral Petrol 105:602-615

Smith HA, Giletti BJ (1997) Lead diffusion in monazite. Geochim Cosmochim Acta 61:1047-1055

Spear FS (1993) Metamorphic Phase Equilibria and Pressure-Temperature-Time Paths. Mineralogical Society of America Monograph, Washington, DC

Spear FS, Parrish RR (1996) Petrology and cooling rates of the Valhalla complex, British Columbia, Canada. J Petrol 37:733-765

Stacey JS, Kramers JD (1975) Approximate of terrestrial lead isotope evolution by a two-stage model. Earth Planet Sci Lett 26:207-221

Stern RA, Berman RG (2000) Monazite U-Pb and Th-Pb geochronology by ion microprobe, with an application to in situ dating of an Archean metasedimentary rock. Chem Geol 172:113-130

Stern RA, Sanborn N (1998) Monazite U-Pb and Th-Ph geochronology by high-resolution secondary ion mass spectrometry. *In* Radiogenic age and isotopic studies, Report 11, Curr Res Geol Surv Canada, Ottawa, 1998-F, p 1-18

Suzuki K, Adachi M (1991) Precambrian provenance and Silurian metamorphism of the Tsunosawa paragneiss in the South Kitakami terrane, northeast Japan, revealed by the chemical Th-U-total Pb isochron ages of monazite, zircon and xenotime. J Geochem 25:357

Suzuki K, Adachi M (1994) Middle Precambrian detrital monazite and zircon from the Hida gneiss on Oki-Dogo Island, Japan: Their implications for the correlation of basement gneiss of Southwest Japan and Korea. Tectonophysics 235:277-292

Suzuki K, Adachi M, Kajizuka I (1994) Electron microprobe observations of Pb diffusion in metamorphosed detrital monazites. Earth Planet Sci Lett 128:391-405

Terry MP, Robinson P, Hamilton MA, Jercinovic, MJ (2000) Monazite geochronology of UHP and HP metamorphism, deformation, and exhumation, Nordoyane, Western Gneiss Region, Norway. Am Mineral 85:1651-1664

Tilton GR (1960) Volume diffusion as a mechanism for discordant lead ages. J Geophys Res 65:2933-2945

Tilton GR, Nicolaysen LO (1957) The use of monazites for age determination. Geochim Cosmochim Acta 11:28-40

Tilton GR, Patterson CC, Brown H, Inghram M, Hayden R, Hess D, Larsen E (1955) Isotopic composition and distribution of lead, uranium and thorium in Precambrian granite (Ontario). Geol Soc Am Bull 66:1131-1148

Townsend KJ, Miller CF, D'Andrea JL, Ayers JC, Harrison TM, Coath CD (2001) Low temperature replacement of monazite in the Ireteba granite, Southern Nevada: geochronological implications. Chem Geol 172:95-112

Van Emden B, Graham J, Lincoln FJ (1997). The incorporation of actinides in monazite and xenotime from placer deposits in western Australia. Can Mineral 35:95-104

Vinogradov AP, Tugarinov AI, Zykov SI, Stupnikova NI, Bibikova YV, Knorre KG, Mel'nikova GL (1966) Geochronology of the Precambrian of India. Akad Nauk SSSR Kom Opred Absol Vozrasta Geol Form Tr 13:394-408

Viskupic K, Hodges KV (2001) Monazite-xenotime thermochronometry: Methodology and an example from the Nepalese Himalaya. Contrib Mineral Petrol 141:233-247

Wang JW, Tatsumoto M, Li X, Permo W, Chao ECT (1994) A precise Th-232-Pb-208 chronology of fine-grained monazite age of the Bayan Obo REE-Fe-Nb ore deposit, China. Geochim Cosmochim Acta 58:3155-3169

Watson EB, Harrison TM, Ryerson FJ (1985) Diffusion of Sm, Sr and Pb in fluorapatite. Geochim Cosmochim Acta 49:1813-1823

Wetherill GW (1956) Discordant Uranium-Lead ages, I. EOS Trans, Am Geophys Union 37:320-326

White NM, Parrish RR, Bickle MJ, Najman YMR, Burbank D, Maithani A (2001) Metamorphism and exhumation of the NW Himalaya constrained by U-Th-Pb analyses of detrital monazite grains from early foreland basin sediments. J Geol Soc 158:625-635

Williams ML, Jercinovic MJ, Terry MP (1999) Age mapping and dating of monazite on the electron microprobe: Deconvoluting multistage tectonic histories. Geology 27:1023-1026

Williams ML, Jercinovic MJ (2002) Microprobe monazite geochronology: Putting absolute time into microstructural analysis. J Struct Geol 24:1013-1028

Willigers BJA, Baker JA, Krogstad EJ, Peate DW (2002) Precise and accurate in situ Pb-Pb dating of apatite, monazite, and sphene by laser ablation multiple-collector ICP-MS. Geochim Cosmochim Acta 66:1051-1066

Wing BA, Ferry JM, Harrison TM (submitted, 2002) Prograde destruction and formation of monazite and allanite during contact and regional metamorphism of pelites: Petrology and geochronology. Contrib Mineral Petrol

Zhu XK, O'Nions RK (1999a) Zonation of monazite in metamorphic rocks and its implications for high temperature thermochronology: A case study from the Lewisian terrain. Earth Planet Sci Lett 171: 209-220

Zhu XK, O'Nions RK (1999b) Monazite chemical composition: Some implications for monazite geochronology. Contrib Mineral Petrol 137:351-363

Zhu XK, O'Nions RK, Belshaw NS, Gibb AJ (1997) Lewisian crustal history from in situ SIMS mineral chronometry and related metamorphic textures. Chem Geol 136:205-218

Zhu XK, O'Nions RK, Gibb AJ (1998) SIMS analysis of U-Pb isotopes in monazite: Matrix effects. Chem Geol 144:305-312